Assimilation of multiple datasets results in large differences in regional to global-scale NEE and GPP budgets simulated by a terrestrial biosphere model

Cédric Bacour[1◎], Natasha MacBean[2], Frédéric Chevallier[1], Sébastien Léonard[1※], Ernest. N. Koffi[1☆], Philippe Peylin[1]

[1] Laboratoire des Sciences du Climat et de l'Environnement, LSCE/IPSL, CEA-CNRS-UVSQ, Université Paris-Saclay, Gif-sur-Yvette, F-91191, France.

[2] Departments of Geography & Environment and Biology, Western University, London, Ontario, Canada.

◎ formerly at NOVELTIS, Labège, France.

※ now at Air Liquide R&D, Innovation Campus Paris - Les-Loges-en-Josas, France.

☆ now at European Centre for Medium-Range Weather Forecasts, Robert-Schuman-Platz 3, 53175 Bonn, Germany.

Correspondance to: Cédric Bacour (cedric.bacour@lsce.ipsl.fr)

Supprimé[cbacour]: **different**

Supprimé[cbacour]: Department of Geography, Indiana University, Bloomington, IN, 47405, USA.

Key Points:

- The impact of assimilating different dataset combinations on regional to global scale C budgets is explored with the ORCHIDEE model
- Assimilating simultaneously multiple datasets is preferable to optimize the values of the model parameters and avoid model overfitting
- The challenges in constraining soil C disequilibrium using atmospheric CO_2 data are highlighted for an accurate prediction of the land sink distribution

Supprimé[Cédric Bacour]: optimizing

Supprimé[Cédric Bacour]: pools

Abstract

In spite of the importance of land ecosystems in offsetting carbon dioxide emissions released by anthropogenic activities into the atmosphere, the spatio-temporal dynamics of terrestrial carbon fluxes remain largely uncertain at regional to global scales. Over the past decade, data assimilation (DA) techniques have grown in importance for improving these fluxes simulated by Terrestrial Biosphere Models (TBMs), by optimizing model parameter values while also pinpointing possible parameterization deficiencies. Although the joint assimilation of multiple data streams is expected to

Supprimé[cbacour]: the

Supprimé[cbacour]: D

Supprimé[cbacour]: A

constrain a wider range of model processes, their actual benefits in terms of reduction in model uncertainty are still under-researched, also given the technical challenges. In this study, we investigated with a consistent DA framework and the ORCHIDEE-LMDz TBM-atmosphere model how the assimilation of different combinations of data streams may result in different regional to global carbon budgets. To do so, we performed comprehensive DA experiments where three datasets (*in situ* measurements of net carbon exchange and latent heat fluxes, space-borne estimates of the Normalized Difference Vegetation Index, and atmospheric CO_2 concentration data measured at stations) are assimilated alone or simultaneously. We thus evaluated their complementarity and usefulness to constrain net and gross C land fluxes. We found that a major challenge in improving the spatial distribution of the land C sinks/sources with atmospheric CO_2 data relates to the correction of the soil carbon imbalance.

Supprimé[Cédric Bacour]: initial

Supprimé[Cédric Bacour]: stocks

1 Introduction

The dramatic growth of atmospheric CO_2 concentrations recorded in the last half-century has increased awareness on the impact of human activities on climate. Taking up about one third of the carbon dioxide from the atmosphere, the terrestrial biosphere plays a key role in regulating CO_2 emissions released by anthropogenic activities (fossil fuel emissions, land use and land cover change) (Friedlingstein et al., 2020). Quantifying variations in the distribution and intensity of carbon (C) sources/sinks from year to year remains a challenge given the complexity of the processes involved and what we can learn from observations. By formalizing current knowledge of the main processes governing the functioning of vegetation into numerical representations, terrestrial biosphere models (TBMs) have grown in importance for studying the spatio-temporal dynamics of net and gross land surface C fluxes from the local to the global scales. However, the large spread in simulated regional to global scale C fluxes for the last few decade (Friedlingstein et al., 2020) as well as for future projections (Arora et al., 2020) highlight the remaining uncertainties in our understanding and prediction of the fate and role of the biosphere under climate change and anthropogenic pressure.

Supprimé[cbacour]: grown

Supprimé[cbacour]: determining

Supprimé[cbacour]: carbon (

Supprimé[cbacour]:)

Supprimé[cbacour]: their

Supprimé[cbacour]: present time

Over the past decade, the parameter uncertainty in TBMs has increasingly been reduced thanks to statistical data assimilation (DA, also referred to as model-data fusion) frameworks, benefiting from the experience gained in other fields of Earth and Environmental sciences (geophysics, weather forecasting, hydrology, oceanography, etc.). DA techniques enable optimization of the model parameters using relevant target observations, while taking into account both observational and modelling uncertainties. DA does not only enable improving the model parameters but can also help

Supprimé[cbacour]: s

Supprimé[cbacour]: ing

pinpointing model deficiencies (Luo et al., 2012). The importance of DA as a key component of terrestrial biosphere carbon cycle modelling is reflected by the diversity of DA systems in the global TBM communities. Since the first global scale Carbon Cycle Data Assimilation System (CCDAS) (Kaminski et al., 2002; Rayner et al., 2005) developed for the Biosphere Energy-Transfer Hydrology (BETHY) model, and in parallel to the development of community assimilation tools (as DART (Anderson et al., 2009) or PECAn (Dietze et al. (2013)), other modelling groups have developed their own global scale carbon cycle DA systems, in particular for ORCHIDEE (ORganizing Carbon and Hydrology In Dynamic EcosystEms model) (Santaren et al., 2007; Peylin et al., 2016), JULES (Joint UK Land Environment Simulator) (Raoult et al. (2016)), JSBACH (Schürmann et al. (2016)), or CLM (Community Land Model) (Fox et al., 2018).

Within a variational DA framework, ground-based measurements of eddy-covariance fluxes at a local scale (Wang et al., 2001; Knorr and Kattge, 2005; Sacks et al., 2007; Williams et al., 2009; Groenendijk et al., 2011; Kuppel et al., 2012) have been widely used to constrain net and gross CO_2 fluxes and latent heat flux. Moreover, remote sensing proxies of vegetation activities, such as raw reflectance data (Quaife et al., 2008), vegetation indices (Migliavacca et al., 2009; MacBean et al., 2015), or FAPAR - fraction of absorbed photosynthetically active radiation (Stöckli et al., 2008; Zobitz et al., 2014; Forkel et al., 2014; Bacour et al., 2015), have also been used to constrain the model parameters at various spatial scales. Finally, atmospheric CO_2 mole fraction measurements have been assimilated to provide valuable information on large-scale net ecosystem exchange (NEE) (Rayner et al., 2005; Koffi et al., 2012).

In the early days of DA studies, most focused on the assimilation of a single data stream (e.g., targetting only NEE). Then, assimilations with multiple different C cycle related datasets have soon been considered (Moore et al., 2008; Richardson et al., 2010; Ricciuto et al., 2011; Keenan et al., 2013; Thum et al., 2017; Knorr et al., 2010; Kaminski et al., 2012; Kato et al., 2013; Bacour et al., 2015; Peylin et al., 2016). The underlying motivation behind assimilating multiple data streams is that using a greater number and diversity of observations should provide stronger constraints on model parameters, including a wider range of processes, hence resulting in a greater reduction in model uncertainty. However, many previous studies that assimilated multiple datasets hardly considered potential incompatibilities between the model and the observations (although see Bacour et al., 2015; Thum et al., 2017), that may result in a deterioration of model agreement with other observations not included in the assimilation. Besides, only a few have quantified the actual benefit of assimilating multiple data-sets compared to the single data stream assimilations, in particular in the context of global scale C cycle DA experiments.

The assimilation of multiple data streams can be done either sequentially, in which one observation type is assimilated at a time, or simultaneously (joint assimilation approach or "batch" strategy as defined in Raupach et al., 2005), where the model is calibrated with all data included in the same optimization (e.g. Richardson et al., 2010; Kaminski et al., 2013; Schürmann et al., 2016). Although with model parameters and observations described by probability distributions, simultaneous and sequential assimilations could theoretically lead to the same result (Tarantola et al. 2005), this is not the case in practice for complex problems. Incomplete or incorrect description of the error statistics may result in large differences between simultaneous and stepwise approaches (see Kaminski et al., 2012; MacBean et al., 2016). In addition, model non linearities also tend to exacerbate these potential differences. Simultaneous assimilation is considered to be more optimal in the context of optimizing TBM parameters as it maximizes the consistency of the model with the whole of the datasets considered (Richardson et al., 2010; Kaminski et al. 2012) and avoid incorrect/incomplete propagation of the error statistics from one step to the other (Peylin et al., 2016). The use of a gradient descent approach for the optimization, with the risk that it gets trapped in local minima, also increases the chances that stepwise and simultaneous approaches diverge. However, sequential approaches remain appealing for modelers: They require less initial technical investment and enable easier assessment of the impact of each data stream assimilated successively onto the optimized variables. Both approaches however face similar challenges, like defining the model-data uncertainty (see, e.g., Richardson et al., 2010; Keenan et al., 2013; Kaminski et al., 2012; Bacour et al., 2015; Thum et al., 2017; Peylin et al., 2016) and hence the weight that each dataset has on the optimization outcome (although specific weighting approaches may be envisioned, as in Wutzler and Carvalhais et al. (2014) or Oberpriller et al. (2021)) . Another major challenge, as highlighted by MacBean et al. (2016) or Oberpriller et al. (2021) , concerns inconsistencies between observations and model outputs, which are usually not accounted for in common bias-blind (Dee, 2005) Bayesian DA systems relying on the hypothesis of Gaussian errors. Indeed, most studies do not attempt to identify systematic errors in the observations and/or in the model and to correct for them. The likely impact of model-data biases on the parameter optimization is then a degraded model performance as well as an illusory decrease in the estimated model uncertainty (Wutzler and Carvalhais, 2014; MacBean et al., 2016; Bacour et al., 2019).

The present study aims to go a step forward in the assessment of how assimilating multiple C cycle related data streams impacts and changes the constraint on net and gross CO_2 flux simulations at the global scale. To do so, we further advance from the sequential assimilation of Peylin et al. (2016) (referred to as "stepwise" approach hereafter) by implementing a simultaneous assimilation framework with the same data streams: net carbon fluxes (net ecosystem exchange – NEE) and

Supprimé[cbacour]: While the latter joint assimilations are more optimal as it maximizes the consistency of the model with the whole of the datasets considered (Richardson et al., 2010),

Supprimé[cbacour]: the

Supprimé[cbacour]: and

Supprimé[cbacour]: of

Supprimé[Cédric Bacour]: (see, e.g., Richardson et al., 2010; Keenan et al., 2013; Kaminski et al., 2012; Bacour et al., 2015; Thum et al., 2017; Peylin et al., 2016)

Supprimé[cbacour]: different

latent heat fluxes (LE) measured at eddy covariance sites across different ecosystems, satellite derived Normalized Difference Vegetation Index (NDVI) at coarse resolution for a set of pixels spanning the main deciduous vegetation types, and monthly atmospheric CO_2 concentration data measured at surface stations worldwide. The study relies on the variational DA framework designed for the ORCHIDEE global vegetation model (Krinner et al., 2005), here associated to a simplified version of the LMDz atmospheric transport model (Hourdin et al., 2006) based on pre-calculated transport fields for assimilating atmospheric CO_2 concentration data. ORCHIDEE and LMDz are the terrestrial and atmospheric components of the IPSL Earth System Model (Dufresne et al., 2013).

By conducting different assimilation experiments in which each data stream is assimilated alone or in combination (for all combinations of datasets), the research questions that we address in this study are:

1. What impact does the combination of different data streams assimilated have on the reduction in model-data misfit, and to which extent are the model predictions improved (or degraded) with respect to the other data-streams that were not assimilated?

2. How does the combination of different data-streams impact the optimised parameter values and uncertainties, and the predicted spatial distribution of the net and gross carbon fluxes at regional and global scales? How do the derived carbon budgets compare with independent process-based model and atmospheric inversion estimates from the Global Carbon Project's 2020 Global Carbon Budget (Friedlingstein et al., 2020)?

3. How does a model–data bias related to incorrect initialisation of soil carbon pools (i.e. their disequilibrium with respect to steady state) impact the overall optimisation performances within a Bayesian assimilation framework relying on the hypothesis of Gaussian errors?

In addition, our analysis of the useful informational content provided by different data-streams on C fluxes is supported by methodological aspects aiming to:

1. Improve the realism of the prior error statistics on parameters by making them consistent with the prior model-data mismatch;

2. Quantify the observation influence of each of the three data streams on the joint assimilation in which all three datasets were included in the optimization.

Mis en forme[cbacour]: Numéros + Niveau: 1 + Style de numérotation: 1, 2, 3, ... + Commencer à: 1 + Alignement: Gauche + Alignement: 0 mm + Retrait: 0 mm

Mis en forme[cbacour]: Puces et numéros

Throughout the presentation of the results, we discuss implications of each assimilation experiment on our ability to accurately constrain gross and net CO_2 fluxes. In the final section we propose some perspectives for other modeling groups wishing to implement global scale parameter DA systems to constrain regional to global scale C budgets.

2 Materials and methods

2.1 Models

2.1.1 ORCHIDEE

Model description

ORCHIDEE is a spatially explicit process-based global TBM (Krinner et al. 2005) that calculates the fluxes of carbon dioxide, water and heat, between the biosphere and the atmosphere, as well as the soil water budget. The temporal resolution is half an hour except for the slow components of the terrestrial carbon cycle (including carbon allocation in plant reservoirs, soil carbon dynamics, and litter decomposition) which are calculated on a daily basis. The version of ORCHIDEE in this study corresponds to that used in the IPSL model for its contribution to the Climate Model Intercomparison Project 5 (CMIP5) established by the World Climate Research Program (https://cmip.llnl.gov/). Vegetation is represented by 13 Plant Functional Types (PFTs) that include bare soil. The processes use the same governing equations for all PFTs, except for the seasonal leaf dynamics (phenology), which follows Botta et al. (2000) (see MacBean et al. (2015) for a full description). The observation operator for NDVI is determined *i)* by assuming a linear relationship between NDVI and FAPAR (Myneni et al., 1994) and *ii)* by calculating FAPAR from the simulated LAI based on the classical Beer-Lambert law for the extinction of the direct illumination within the canopy (Bacour et al., 2015 ; MacBean et al., 2015). In addition, we consider normalized data in our assimilation scheme. The soil organic carbon is simulated by a CENTURY-type model (Parton et al., 1987) and is partitioned in three pools (slow, passive, active) with different residence times.

Model Set-up

The set-up of the simulations performed with ORCHIDEE depends on the data assimilated. The model is run at site scale for the assimilation of eddy-covariance measurements, at spatial resolution 0.72° for the assimilation of the satellite NDVI data, and at the resolution of the atmospheric transport model LMDz (3.75°x2.5°) for the assimilation of atmospheric CO_2 measurements. The Olson land cover classification at 5 km is used to derive the PFT fractions at each spatial resolution, but for the flux tower simulations where the proportion of each PFT is set based on expert knowledge. For satellite pixels and global simulations, ORCHIDEE is forced using the 3-hourly ERA-Interim gridded meteorological forcing fields (Dee et al., 2011) (aggregated at 3.75°x2.5° when assimilating

Supprimé[Cédric Bacour]: As a preliminary step, we tuned prior and observation error statistics: we enhanced their realism by making them consistent with the differences between prior model simulations and observations. We then conducted different assimilation experiments in which each data stream was assimilated alone on in combination (for all combinations of datasets) to assess what the impact of each assimilation experiment was on: a) the fit to each dataset (including datasets included and excluded from the assimilations); b) on the resultant regional to global scale gross and net CO_2 flux budget (NEE and GPP); and c) on the optimized parameter values and uncertainties. We complemented our analysis by comparing our regional to global scale C budgets with independent process-based model and atmospheric inversion estimates from the Global Carbon Project's 2020 Global Carbon Budget (Friedlingstein et al., 2020).

Supprimé[Cédric Bacour]:

Supprimé[Cédric Bacour]: We completed our assessment of the impact of each assimilation scenario by quantifying the observation influence of each of the three data streams on the joint assimilation in which all three datasets were included in the optimization. By determining the overall constraint brought by each data set on the inversion, this final analysis allowed us to highlight the importance of atmospheric CO_2 data in the optimisation of soil C pools despite the smaller number of observations assimilated. Throughout the presentation of the results, we discuss implications of each assimilation experiment on our ability to accurately constrain gross and net CO_2 fluxes. In the final section we propose some perspectives for other modeling groups wishing to implement global scale parameter DA systems to constrain regional to global scale C budgets.

Supprimé[Cédric Bacour]: as in MacBean et al., 2015

atmospheric CO_2 concentrations). For the flux tower simulations, the model is forced by local measurements of the meteorological variables at a half-hourly time step.

For each spatial resolution, a prior spin-up simulation was performed by recycling available forcing data. The objective was to bring the different soil carbon reservoirs to "realistic" values, albeit the spin-up runs result in neutral net carbon flux by construction. Each spin-up simulation was then followed by a transient simulation (starting from the first year of measurement for each data stream) and accounting for the secular increase of atmospheric CO_2 concentrations; for the global simulations, only a short transient simulation from 1990 to 1999 is performed.

2.1.2 LMDz

Model description

The study relies on version 3 of the Atmospheric General Circulation Model of the Laboratoire de Météorologie Dynamique (LMDz) (Hourdin et al., 2006) as implemented for the IPSL contribution to CMIP4. In order to save computational time, we used LMDz in the form of a precomputed Jacobian matrix at a set of CO_2 measurement stations (§2.2.3) (see details in Peylin et al., 2016).

Model set-up

To simulate atmospheric CO_2 concentrations that can be compared to observations, the transport model has to be forced not only by terrestrial biospheric fluxes (calculated by ORCHIDEE), but also by other natural (e.g. ocean) and anthropogenic CO_2 fluxes. We imposed a net emission due to land use change (i.e. deforestation) of 1.1 $GtC.yr^{-1}$ although we also accounted for a larger flux from biomass burning but compensated partly by forest regrowth (see Peylin et al. (2016) for more details). The global maps of biomass burning emissions were taken from the Global Fire Emission Database version 3 dataset (Van der Werf et al., 2006; Randersen et al., 2013) over the period 1997-2010 at a monthly time step and gridded at 0.5°x0.5° resolution. The global fossil fuel CO_2 emission products used here were developed by University of Stuttgart/IER based on EDGAR v4.2 and were provided at a 0.1°x0.1° spatial resolution and at a monthly time scale. The ocean flux component was obtained from a data-driven statistical model based on artificial neural networks that estimated the spatial and temporal variations of the air-sea CO_2 fluxes (Peylin et al., 2016).

2.2 Assimilated data

2.2.1 in situ *flux measurements (F)*

The NEE and LE measurements come from the FLUXNET global network. We used harmonized, quality-checked and gap-filled data (Level 4) at 68 sites from the La Thuile global synthesis dataset (Papale, 2006). The site locations are presented in Figure 1. These ecosystem measurements cover very different time spans, ranging from one single year at some sites up to nine years. They constrain seven PFTs among the twelve natural vegetation types represented in ORCHIDEE: tropical evergreen broadleaf forest – TrEBF (3 sites corresponding to 6 site-years), temperate evergreen needleleaf forest – TeENF (16 sites, 45 sites-years), temperate evergreen broadleaf forest – TeEBF (2 sites, 4 site-years), temperate deciduous broadleaf forest – TeDBF (11 sites, 37 site-years), boreal evergreen needleleaf forest – BoENF (12 sites, 44 site-years), boreal deciduous broadleaf forest – BoDBF (3 sites, 6 site-years), and C3 grassland – C3GRA (21 sites, 56 site-years). We assimilated daily-mean values of NEE and LE observations, but only when at least 80% of the 48 potential half-hourly data in a day are available.

Supprimé[Cédric Bacour]: is

2.2.2 *Satellite products (VI)*

The NDVI products considered here are derived from MODIS collection 5 surface reflectance data acquired in the red and near-infrared channels and corrected from the directional effects (Vermote et al. (2009). The daily data at 0.72° spanning the period 2000-2010 already assimilated into ORCHIDEE and described in MacBean et al. (2015) are considered. Five among the six deciduous, non-agricultural, PFTs of ORCHIDEE were optimized in this study: TrDBF - tropical broadleaved rainy green forest, TeDBF, BoDBF, BoDNF – Boreal needleleaf summergreen forest, and C3GRA. C4 grasses and evergreen PFTs were not considered. For each PFT, fifteen 0.72° pixels were selected for assimilation depending on their thematic homogeneity with respect to the considered PFT (fractional coverage above 60%) and consistency between the observed NDVI time series and the prior ORCHIDEE. The location of these satellite pixels is shown in Figure 1.

2.2.3 *Atmospheric CO_2 measurements (CO2)*

The surface atmospheric CO_2 concentration data come from three databases: The NOAA Earth System Laboratory (ESRL) archive (ftp://ftp.cmdl.noaa.gov/ccg/co2/), the CarboEurope IP project (http://ceatmosphere.lsce.ipsl.fr/database/index_database.html), and the World Data Centre for Greenhouse Gases of the World Meteorological Organization Global Atmospheric Watch Programme (http://gaw.kishou.go.jp). The data include *in situ* measurements, made by automated quasi-continuous analysers, and air samples collected in flasks and later analyzed at central facilities. In this

study, we used monthly-mean values of these measurements (Peylin et al., 2016). Ten years of observations over the 2000-2009 period were used from a total of 53 stations located around the world (Figure 1).

2.3 Assimilation methodology

2.3.1 Data assimilation framework

The data assimilation system associated to the ORCHIDEE model (ORCHIDAS) has been described in previous studies regarding the assimilation of these data streams alone (Kuppel et al., 2012; Santaren et al., 2014; MacBean et al., 2015; Bastrikov et al., 2018) or their combinations (Bacour et al., 2015; Peylin et al., 2016). The assimilation system relies on a variational Bayesian framework that optimizes ORCHIDEE parameters gathered in a vector **x**, by finding the minimum of a global misfit function $J(\mathbf{x})$ iteratively. $J(\mathbf{x})$ is a linear combination of the misfit functions associated with each data stream. It is assumed that the errors of observations and on the model parameters are Gaussian and that the data streams errors are independent from each other:

$$J(\mathbf{x}) = \frac{1}{2}[(H_{LMDz}\circ H_{ORCH}(\mathbf{x}) - \mathbf{y^{CO2}})^{T}.\mathbf{R^{-1}_{CO2}}.(H_{LMDz}\circ H_{ORCH}(\mathbf{x}) - \mathbf{y^{CO2}}) + (H_{ORCH}(\mathbf{x}) - \mathbf{y^{F}})^{T}.\mathbf{R^{-1}_{F}}.(H_{ORCH}(\mathbf{x}) - \mathbf{y^{F}}) + (H_{ORCH}(\mathbf{x} - \mathbf{y^{VI}}))^{T}.\mathbf{R^{-1}_{VI}}.(H_{ORCH}(\mathbf{x}) - \mathbf{y^{VI}}) + (\mathbf{x} - \mathbf{x^{b}})^{T}.\mathbf{B^{-1}}.(\mathbf{x} - \mathbf{x^{b}})] \quad (1)$$

where $\boldsymbol{y^o}$ are the observation vectors (with *o* = *F (flux)*, *VI (satellite NDVI)*, or CO_2 (concentration); H_{ORCH} and H_{LMDz} are the observational operators of the ORCHIDEE and LMDz models, respectively. $\mathbf{R^o}$ is the error covariance matrix characterizing the observation errors with respect to the model (therefore including the uncertainty in the model structure) associated to data stream *o*. The dimensionless control vector $\boldsymbol{\chi}$ quantifies the distance between the values of the optimized parameters and the corresponding prior information $\boldsymbol{x^b}$: $\boldsymbol{\chi} = \boldsymbol{B^{-1/2}}.(\boldsymbol{x} - \boldsymbol{x^b})$, where **B** is the associated *a priori* error covariance matrix.

We use the gradient-based L-BFGS-B algorithm (Byrd et al., 1995; Zhu et al., 1997) to minimize $J(\boldsymbol{x})$ iteratively. It accounts for bounds in the parameter variations. The algorithm requires the gradient of the misfit function as an input in order to explore the parameter space:

$$\nabla_x J(x) = \mathbf{H^{CO2}_{ORCH}}^{T}.\mathbf{H_{LMDz}}^{T}.\mathbf{R^{-1}_{CO2}}.(H_{LMDz}\circ H_{ORCH}(\mathbf{x}) - \mathbf{y^{CO2}}) + \mathbf{H^{F}_{ORCH}}^{T}.\mathbf{R^{-1}_{F}}.(H_{ORCH}(\mathbf{x}) - \mathbf{y^{F}}) + \mathbf{H^{VI}_{ORCH}}^{T}.\mathbf{R^{-1}_{VI}}.(H_{ORCH}(\mathbf{x}) - \mathbf{y^{VI}}) + B^{-1}.(\mathbf{x} - \mathbf{x^{b}}) \quad (2)$$

Supprimé[Cédric Bacour]: ORCHIDEE model

Mis en forme[cbacour]: Police: （Default）DejaVu Math TeX Gyre

Supprimé[cbacour]: <math>

Mis en forme[cbacour]: Police: （Default）DejaVu Math TeX Gyre, Pas Italique

Mis en forme[cbacour]: Police: （Default）DejaVu Math TeX Gyre, Pas Italique

Mis en forme[cbacour]: Police: （Default）DejaVu Math TeX Gyre, Pas Italique

Mis en forme[cbacour]: Police: （Default）DejaVu Math TeX Gyre

Supprimé[cbacour]: <math>

Mis en forme[cbacour]: Police: （Default）DejaVu Math TeX Gyre

Supprimé[cbacour]: <math>

Mis en forme[cbacour]: Police: （Default）DejaVu Math TeX Gyre

Supprimé[cbacour]: <math>

Supprimé[cbacour]: <math>

Mis en forme[cbacour]: Anglais(États-Unis)

Supprimé[cbacour]: <math>

Supprimé[cbacour]: <math>

The calculation of $\nabla_x J(\mathbf{x})$ uses the Jacobian matrix of ORCHIDEE associated to each data stream, $\mathbf{H}^{\mathbf{o}}_{\mathbf{ORCH}}$ (assuming local linearity of the model), and that of LMDz. For most of ORCHIDEE parameters, $\mathbf{H}^{\mathbf{o}}_{\mathbf{ORCH}}$ is calculated thanks to the tangent linear model of ORCHIDEE obtained by automatic differentiation using the TAF (Transformation of Algorithms in Fortran) tool (Giering et al., 2005); however, for a few parameters involved in threshold conditions of the model processes, especially related to phenology, we use a finite difference method.

After optimization, the posterior error covariance matrix **A** (for "analysis") of the optimized parameters can be calculated as a function of the Jacobian matrix associated to the gradients of the model outputs with respect to the parameters at the solution for each data stream:

$$\mathbf{A} = \left[\sum \quad \mathbf{H_o}^{\mathrm{T}} . \mathbf{R_o^{-1}} . \mathbf{H_o} + \mathbf{B}^{-1} \right]^{-1} \qquad (3)$$

It is computed under the hypothesis of model linearity in the vicinity of the solution. The square root of the diagonal elements of **B** or **A** correspond to the standard deviation σ on model parameters.

2.3.2 *Parameters to be optimized*

We chose to optimize a limited set of carbon-cycle related parameters of ORCHIDEE as a result of preliminary sensitivity analyses and past DA studies. A short definition of these parameters that mostly control photosynthesis, phenology and respiration, is provided in Table 1, while their associated prior values, bounds and uncertainty are documented in Supplementary Table S3. More comprehensive descriptions of their role in the model processes are provided in Kuppel et al. (2012) and MacBean et al. (2015). The size of soil carbon pools drives the magnitude of the net carbon fluxes exchanged with the atmosphere to a large extent; Soil carbon is closely related soil texture, climatic (temperature and moisture), disturbance history (including land use and fires), as well as ecosystem and edaphic properties (Schimel et al., 1994; Todd-Brown et al., 2013). Given that we do not have access to that information, neither at the site scale (for assimilation of NEE measurements) nor at the global scale (for assimilation of atmospheric CO_2 concentrations), we use a steady state assumption where ORCHIDEE has been brought to near equilibrium with a long spin-up of the soil carbon pools. To correct for this bias, the initial state of the soil carbon reservoirs is optimized using a multiplicative parameter of both the slow and passive pools as in Peylin et al.(2016). The use of these correction factors is a handy way to correct any issues related to the use of our soil organic C model and the soil carbon disequilibrium. Two multiplicative parameters are used depending on the type of

Mis en forme[cbacour]: Police: （Default）DejaVu Math TeX Gyre

Mis en forme[cbacour]: Police: （Default）DejaVu Math TeX Gyre, Gras, Pas Italique

Mis en forme[cbacour]: Police: （Default）DejaVu Math TeX Gyre

Mis en forme[cbacour]: Police: （Default）DejaVu Math TeX Gyre, Gras, Pas Italique

Mis en forme[cbacour]: Police: （Default）DejaVu Math TeX Gyre

Mis en forme[cbacour]: Police: （Default）DejaVu Math TeX Gyre

Mis en forme[cbacour]: Police: Gras, Pas Italique

Mis en forme[cbacour]: Police: Gras, Pas Italique

Supprimé[cbacour]: <math>

Supprimé[Cédric Bacour]: and

Supprimé[Cédric Bacour]: to the land use history

data considered (and their associated spatial scale): for *in situ* flux measurements, we considered site-specific parameters $K_{soilC,site}$; for atmospheric CO_2 concentration data, instead of resolving the initial conditions for all LMDz grid cells we scaled the carbon pools for 30 large scale regions $K_{soilC,reg}$. Note that having correct soil carbon pools is less important when assimilating satellite NDVI data because these are more closely related to carbon uptake rather than net carbon flux. In total, up to 182 parameters are optimized depending on the data streams considered.

The prior values $\mathbf{x}^b$ of the parameters are set to the standard values of ORCHIDEE (Supplementary Table S3). Not all parameters are constrained by all three data streams. In particular, satellite FAPAR/NDVI products inform the timing of phenology of plant vegetation (start and end of the growing season) rather than on photosynthesis or respiration with our DA system (Bacour et al., 2015; MacBean et al., 2015). The dependency of each parameter with respect to the assimilated data streams is indicated in Table 1.

Mis en forme[cbacour]: Police: Pas Italique

2.3.3 Data assimilation experiments

Different data assimilation experiments were tested in order to understand the respective constraint brought by each data stream and evaluate their compatibility with each other and with the model. First, each data stream was assimilated separately and then its combinations with the other two were considered. Second, the three data streams are assimilated altogether. The various experiments are described in Table 2 with the number of data points assimilated and the number of parameters optimized. Indeed, the number of optimized parameters differs with the type of data assimilated as described in §3.2 and in Table 1. The assimilations have a high computational cost, with an average value for joint assimilations using all three data streams of about 50,000 hr Central Processing Unit time on AMD Rome compute nodes at 2.6 GHz with 256 GB memory per node.

Two assimilation experiments combining the three data streams were tested: one experiment (F+VI+CO2) with all parameters optimized in a single step; and an additional experiment following a 2-step optimization (F+VI+CO2-2steps), as described hereafter. In the first step, the global soil carbon reservoirs are constrained by assimilating atmospheric CO_2 data only, and optimizing the two main parameters controlling soil respiration, $KsoilC_{reg}$ and *Q10*. In the second step, all parameters but $KsoilC_{reg}$ were optimized from the three data streams: $KsoilC_{reg}$ was retained from the first step and *Q10* was optimized but the prior uncertainty for *Q10* for the second step corresponded to the posterior uncertainty derived from the first step. We did this to correct for the initialisation of the soil carbon imbalance following model spin-up and illustrate how the informational content of the three data-streams relative to the surface carbon fluxes can be enhanced once soil carbon

Supprimé[Cédric Bacour]: pools

disequilibrium is more "realistically" represented; the motivations and implications of the two assimilations experiments are further discussed in the result and discussion sections.

The results of these assimilations were compared to the companion study of Peylin et al. (2016) in which the same data streams were assimilated in a sequential/stepwise approach: NDVI data were assimilated first, then *in situ* flux measurements, and finally atmospheric CO_2 concentration measurements. While only 3 years of atmospheric CO_2 data were used in Peylin et al. (2016), the stepwise results presented here really accounts for the same ten years used in the simultaneous experiments (2000-2009) to facilitate the comparison of the approaches (in particular the impact of using the atmospheric CO_2 growth rate over 10 years on the optimisation of the mean terrestrial carbon sink). There are however a few differences in the set-up compared to the present study (cf. details provided in Supplementary Text S1).

Mis en forme[cbacour]: Indice

Supprimé[Cédric Bacour]: In addition, t

Supprimé[Cédric Bacour]: , in particular the use of only three years of atmospheric CO2 data

2.3.4 Error statistics on observations and parameters

2.3.4.1 Observation error statistics

Like in previous studies with ORCHIDAS, we defined **R** as diagonal and computed the variances from the Root Mean Square Difference (RMSD) between the data and the *a priori* ORCHIDEE simulations (*i.e.* performed with the model default parameter values) for fluxes and satellite observations. However, it is worth noting that this approach overestimates the variances in order to compensate for any neglected correlations. For atmospheric CO_2 measurements, we followed a different methodology given the large discrepancy in the modelled *a priori* concentrations with respect to the observed data (i.e., large bias that increases over time due to biases in the land net carbon sink (too small)). The errors were determined at each site as the standard deviation of the observed temporal concentrations (Peylin et al., 2005, 2016), to capture the general feature that model-data mismatch is likely large for sites and months with large variations in daily concentrations. Although crude, such an hypothesis has been used in many atmospheric CO_2 inversions and in our case it combines all structural errors of the terrestrial and transport models.

Mis en forme[cbacour]: Police: Italique

Mis en forme[cbacour]: Indice

Supprimé[cbacour]: : the errors were determined as a function of the observed and modelled temporal concentration variability at each site (Peylin et al., 2016), thus neglecting the structural errors of the terrestrial model.

2.3.4.2 Tuning of the prior error statistics

We assumed that errors in the prior parameter values are independent and therefore we used a diagonal **B** matrix. We populated the diagonal of **B** in an iterative way from consistency diagnostics of the data assimilation system following Desroziers et al. (2005), as described hereafter. If both **B** and **R** matrices are correctly specified and if the estimation problem is linear, they should be related to the

covariance of the residuals (**d**) between observations and background simulations (*i.e.* innovation) following:

$$\mathbf{H_o}.\mathbf{B}.\mathbf{H_o}^{\mathrm{T}} + \mathbf{R} = E\left[(\mathbf{y^o} - H(\mathbf{x^b})).(\mathbf{y^o} - H(\mathbf{x^b}))^{\mathrm{T}}\right] = E\left[\mathbf{d_b^o}.\mathbf{d_b^{o\mathrm{T}}}\right] \quad (4)$$

With

$$\mathbf{R} = E\left[(\mathbf{y^o} - H(\mathbf{x^a})).(\mathbf{y^o} - H(\mathbf{x^b}))^{\mathrm{T}}\right] = E\left[\mathbf{d_a^o}.\mathbf{d_b^{o\mathrm{T}}}\right] \quad (5)$$

$$\mathbf{H_o}.\mathbf{B}.\mathbf{H_o}^{\mathrm{T}} = E\left[(H(\mathbf{x^a}) - H(\mathbf{x^b})).(\mathbf{y^o} - H(\mathbf{x^b}))^{\mathrm{T}}\right] = E\left[\mathbf{d_b^a}.\mathbf{d_b^{o\mathrm{T}}}\right] \quad (6)$$

Similarly, the diagnostic on analysis errors can be determined from the residuals between observations and posterior simulations as:

$$\mathbf{H_o}.\mathbf{A}.\mathbf{H_o}^{\mathrm{T}} = E\left[(H(\mathbf{x^a}) - H(\mathbf{x^b})).(\mathbf{y^o} - H(\mathbf{x^a}))^{\mathrm{T}}\right] = E\left[\mathbf{d_b^a}.\mathbf{d_a^{o\mathrm{T}}}\right] \quad (7)$$

In principle, the tuning of **B** and **R** needs to be performed iteratively for successive values of $\mathbf{x^a}$ and of the corresponding residuals, until convergence, which is prohibitive in terms of computing time. The estimation of the covariance matrices depends on the mathematical expectation (*E*) which would require several realizations of the residuals to diagnose the error statistics (Desroziers et al. (2005); Cressot et al., 2014). In this study, only one optimization was performed using one set of *a priori* parameters for each dataset. We therefore calculated these metrics by averaging the diagonals of the matrices described by both sides of the equations for all available observations (Kuppel et al., 2013). This way, both sides are scalar values (Cressot et al., 2014).

The standard deviation of the errors were determined after a few trials considering the three single data stream assimilation experiments independently: For each DA experiment we started from an initial parameter error set at 40% of the variation interval for each parameter (as in Peylin et al., 2016); The errors were then varied in order to fulfill the consistency diagnostics on the parameter and observation errors (see Supplementary Text S3). Finally, we evaluated the consistency of the resulting model-data covariance matrices for the DA experiments with multiple data streams using the reduced chi-square test (i.e. the chi-square statistic normalized by the number of observations, *m* (Chevallier et al., 2007; Klonecki et al., 2012), which is implicitly optimized by the Desroziers et al. (2005) approach:

$$\chi^2 = \frac{2J(\mathbf{x^a})}{m} \quad (8)$$

Supprimé[cbacour]: <math>

Supprimé[cbacour]: <math>

Supprimé[cbacour]: <math>

Supprimé[cbacour]: <math>

Supprimé[cbacour]: <math>

Supprimé[cbacour]: <math>

Supprimé[cbacour]: <math>

Supprimé[cbacour]: <math>

Supprimé[cbacour]: <math>

Supprimé[cbacour]: <math>

Mis en forme[cbacour]: Police: （Default）DejaVu Math TeX Gyre, Gras, Pas Italique

Mis en forme[cbacour]: Police: （Default）DejaVu Math TeX Gyre

Mis en forme[cbacour]: Police: （Default）DejaVu Math TeX Gyre, Gras, Pas Italique

Mis en forme[cbacour]: Police: （Default）DejaVu Math TeX Gyre

If the **R** and **B** covariance matrices are well defined, the ratio of each term of the diagnostics of Desroziers et al. (2005) (ratio between **R** and $E\left[\mathbf{d_a^o}.\mathbf{d_b^o}^{\mathrm{T}}\right]$; $\mathbf{H_o}.\mathbf{B}.\mathbf{H_o}^{\mathrm{T}}$ and $E\left[\mathbf{d_b^a}.\mathbf{d_b^o}^{\mathrm{T}}\right]$; and $\mathbf{H_o}.\mathbf{B}.\mathbf{H_o}^{\mathrm{T}}+\mathbf{R}$ and $E\left[\mathbf{d_b^o}.\mathbf{d_b^o}^{\mathrm{T}}\right]$) should approach 1. Table 3 shows the values of the consistency diagnostics for the final parameter error set-up.

The diagnostics for **R** (ratios slightly above 1 for all data streams**)** and for the reduced chi-square (Table S1 - values below 1) indicates a slight overestimation of the observation error. The diagnostics for **B** (*ratio*^{B}) show a stronger overestimation of the *a priori* error for NEE, LE and atmospheric CO_2, but an underestimation for NDVI. For fluxes and satellite data, the combined diagnostics for **R** and **B** (*ratio*^{BR}) appear consistent with ratios close to 1. For CO2 however, the value of *ratio*^{BR} close to the value of *ratio*^{B} highlights the strong influence of the background information (**B** matrix) or the model structure on the optimization, while the large value of χ^2 expresses a strong underestimation of the observation error. Indeed, when determining $\mathbf{R_{CO2}}$, we purposely did not account for the large bias (by about 1 ppm.yr^{-1}) between the observed CO_2 temporal profiles at stations and the prior simulations, which is due to the initialisation of ORCHIDEE's carbon pools (which is discussed in the Result section). Finally, for the diagnostics on the analysis, the various tests performed (Supplementary Text S3) all lead to negative quantities. Instead, the simulations of the calibrated model were expected to be contained in between their prior state and the observations (the residuals having opposite signs, their product is positive). This result may reflect a too strong model correction. However, it should be noted that a strong assumption associated with these tests concerns the linearity of the model, which may not hold for terrestrial biosphere models.

2.4 Diagnostics for system evaluation

2.4.1 Optimisation performance

We measured the efficiency of any assimilation by quantifying the reduction of the cost function as the ratio of the prior to posterior values. It should be noted that the minimum value of the cost function is not expected to be zero given the uncertainty in both the data and model, and the limited number of degrees of freedom (number of optimized parameters) allowed. We also looked at the ratio of the norm of the gradient between the prior and posterior misfit functions, as it illustrates the progression towards the expected optimum, for which the gradient is null. The decrease of the norm of the gradient depends on the estimation problem (non-linearities, number of observations versus number of optimized parameters, constraints of the data on the model processes, etc.); however, based on our experience with non-linear problems, we still expect the norm of the gradient to be reduced by at least two orders of magnitude.

Supprimé[cbacour]: <math>
Supprimé[cbacour]:
Mis en forme[cbacour]: Police: Gras, Pas Italique
Mis en forme[cbacour]: Police: Gras, Pas Italique
Mis en forme[cbacour]: Police: Gras, Pas Italique
Mis en forme[cbacour]: Police: Gras, Pas Italique
Mis en forme[cbacour]: Police: Gras, Pas Italique
Mis en forme[cbacour]: Police: Gras, Pas Italique
Mis en forme[cbacour]: Police: Pas Italique
Supprimé[cbacour]: <math>
Supprimé[cbacour]: <math>
Supprimé[cbacour]: <math>
Supprimé[cbacour]: <math>
Mis en forme[cbacour]: Police: （Default）DejaVu Math TeX Gyre

The analysis of the optimization performances are summarized in §3.1 and detailed in Supplementary Text S4.

2.4.2 Model improvement and posterior predictive checks

The model improvement was quantified by the reduction of the root mean square deviation (RMSD) between model and data, prior and posterior to optimization, expressed in %, as $100 \times (1 - \frac{RMSD_{post}}{RMSD_{prior}})$.

We conducted posterior predictive checks by running the model optimized after assimilation of one or two data streams and quantifying the resulting model-improvement with respect to the data streams not accounted for in the assimilation.

2.4.3 Uncertainty reduction on parameters and error budget

The knowledge improvement on the model parameters brought by assimilation was assessed by the uncertainty reduction determined by 1- $\sigma_{post}/\sigma_{prior}$, where σ_{post} and σ_{prior} are the standard deviation derived from the posterior (**A**) and prior (**B**) covariance matrices on the model parameters and output variables.

A comprehensive quantification of the uncertainty reduction on model variables would require accounting also for the covariance matrix of the model structural error which could be the dominant factor. Because this covariance matrix is difficult to estimate for complex process-based terrestrial biosphere models (see Kuppel et al., 2013, for a first attempt in the case of the NEE), we instead analyzed the posterior errors on NEE and GPP at regional to global scales, as the projection of the posterior error on parameters in the space of the model variables. The posterior error on C fluxes is then characterized by the covariance matrix $\mathbf{R^a}$ as:

$$\mathbf{R^a} = \mathbf{H_o} . \mathbf{A} . \mathbf{H_o}^{T} \quad (9)$$

Supprimé[cbacour]: <math>

with the Jacobian matrix $\mathbf{H_o}$, being the first derivative of the target quantity (e. g., NEE, GPP) to the optimized parameters derived from an assimilation experiment *o*.

2.4.4 Assessment of the information content of each data stream

For the joint assimilations using the three di fferent data streams, we further analyzed the influence matrix **S** that quantifies their leverage on the model-data fit (Cardinali et al., 2004):

$$\mathbf{S} = \mathbf{R}^{-1} . \mathbf{H} . \mathbf{A} . \mathbf{H}^{T} \quad (10)$$

Supprimé[cbacour]: <math>

A diagonal element S_{ii} is the rate of change of the simulated observable *i* with respect to variations in the corresponding assimilated observation *i*. S_{ii} is referred to as "self-sensitivity" of "self-influence". A zero self-sensitivity indicates that this i^{th} observation does not contribute to improving its simulation by the model, whilst $S_{ii} = 1$ indicates that the fit of the sole observation *i* mobilizes an entire degree of freedom (*i.e.* one parameter). In addition to the total influence matrix (equation 10), we also determined the partial influence matrices associated to each data stream *o*, using the corresponding diagonal $\mathbf{R_o}$ matrices and $\mathbf{H}$ in equation 10.

We analyzed the trace (i.e. the sum of all diagonal elements) of **S** that quantifies a measure of the amount of information that can be extracted from all observations / all data streams. We used two derived quantities: the global average observation influence (OI) and the relative degrees of freedom for signal (DFS) associated with the data stream *o,* which measures its relative contribution to the fit. They are defined as follow (with *m* the total number of observations):

$$OI = \frac{tr(\mathbf{S})}{m} \tag{11}$$

and

$$DFS = 100 \times \frac{tr(\mathbf{S_o})}{tr(\mathbf{S})} \tag{12}$$

3 Results

Supprimé[Cédric Bacour]: **and discussion**

3.1 Model improvement for the different assimilation experiments

3.1.1 Cost function reduction

The reduction of the cost function varies between the different experiments with the lowest reductions for the single data streams experiments F and VI (around 10%). However, the correction of the model-data misfit when CO_2 data are assimilated is much higher (at least factor of 10 reduction). Noteworthy, this strong model improvement is obtained for a lower departure of the parameters from their prior values than when fluxes or satellite data are assimilated (cf. section 3.3, and Figure 6).

A detailed description of the optimization performances with respect to the minimisation of the cost function is detailed in Supplementary Text S4 and Table S2.

3.1.2 Overall fit to the observations

The impact of assimilating one type of observation on all the data streams (including those that are not assimilated) was evaluated for the various assimilation experiments. The reduction of the model-data mismatch (i.e. reduction in prior RMSD) after assimilation of each data stream (or any

combination of them) is illustrated in Figure 2. The length of the boxes (first and third quartiles) of the whisker plots highlight the spread in misfit reduction across sites/vegetation types. For fluxes, only the impact on NEE is shown, given the choice of optimizing parameters is mostly related to the carbon cycle. Using the parameter values optimized in either the F and VI assimilations has a strong detrimental impact on the simulated atmospheric CO_2 data because the soil carbon pools were not adjusted in these DA experiments. Therefore, we also analyzed the changes induced on the detrended seasonal cycles of atmospheric CO_2 concentrations (hence removing the trend using the time series decomposition based on the CCGCRV routine (Thoning et al., 1989), as described in Supplementary Text S2) (Figure 2c).

For a given data stream, the improvement is usually better for the experiment where that data stream is assimilated alone. One noteworthy exception is the assimilation of NDVI alone (VI experiment where only the phenology parameters are optimized) that results in a lower model improvement with respect to NDVI than when it is assimilated in combination with other data-streams (where a higher number of parameters are optimized in these joint assimilations, hence improving the timing of phenology and the amplitude of the annual cycle when flux or atmospheric CO2 data are also assimilated). For both experiments F and VI, the reduction of the model-data misfit can be negative, which reflects how the assimilation can degrade the model performance for a few pixels/sites by searching for a common parameter set. This is not observed with the assimilation of atmospheric CO_2 data only for which the optimized model is always closer to the observations than the prior model (due to a correction of the CO_2 trend), at all stations (see Supplementary Text S5 for a detailed description of the reduction in model-data misfit each single-data stream assimilation experiment (F, VI, CO2)).

Supprimé[Cédric Bacour]: (compared to joint assimilation of two or more data streams; Figure 2).

Supprimé[Cédric Bacour]: . Only the phenology parameters are optimized with NDVI alone. In contrast,

Supprimé[cbacour]: se

Supprimé[cbacour]: involving NDVI

Supprimé[cbacour]: which

Supprimé[Cédric Bacour]: es

The collateral impact of assimilating one data stream on the other simulated observables is evident in the misfit reductions shown in Figure 2 (e.g., examine the “VI” experiment on the NEE misfit reduction in Figure 2a). While using optimized phenological parameters retrieved from satellite data alone (experiment VI) degrades the modelled seasonality of NEE as compared to the measurements (median RMSD reduction of -3%), the optimization with respect to *in situ* flux data (F), with additional control parameters, leads to a general improved consistency between modelled FAPAR and satellite NDVI time series (median RMSD reduction of 8%). The impact on LE is much lower for all DA experiments (median values close to 0% in all cases, result not shown). One can also note the positive impact of the F and VI assimilations on the atmospheric CO_2 data with median RMSD reductions of 15.8% and 11.2% respectively for the detrended time series. Such an improvement after assimilation of *in situ* flux data corroborates the findings of Kuppel et al. (2014) and Peylin et al.

(2016). Noteworthy, this improvement is of the same order as that achieved when assimilating atmospheric CO_2 data alone (median RMSD reduction of 14%). The parameters retrieved from the CO2 experiment have also a small but positive impact at the site level with respect to NEE (median value of 3%) and FAPAR (0.8%).

For the joint assimilation experiment (F+VI, F+CO2, VI+CO2, or F+VI+CO2; Figure 2), the model-data agreement is improved for all assimilated data streams, as expected, while the model degradation relative to the data not assimilated is generally not as severe as compared to the assimilation of individual data stream experiments described above, with the exception of the F+VI experiment. The latter experiment leads to enhanced model improvement compared to when flux and satellite NDVI data are assimilated alone (cf. Supplementary Text S5). In the simultaneous assimilations involving atmospheric CO_2 data, most of the model improvement concerns CO2 (Figure 2c) while the benefit for the fluxes and FAPAR/NDVI is weak (RMSD reduction below 3%). Noteworthy, the 2-step assimilation F+VI+CO2 (see Section 2.3.3) results in an even higher model improvement for both NEE and FAPAR than the 1-step approach.

Supprimé[Cédric Bacour]: These low values are explained by the fact that, in the CO2 assimilation, most of the model improvement is attributable to

Supprimé[Cédric Bacour]: simultaneous assimilation of flux measurements and satellite NDVI data (F+VI)

The misfit reduction for the raw (i.e., not detrended) atmospheric CO_2 data is high (median reduction ~75%) and remains quite stable among the various different combinations of data streams that include atmospheric CO2 (Figure 2c solid bars experiments including "CO2"), with the exception of the F+VI+CO2-2steps experiments. The misfit reductions for the detrended CO_2 time series are generally lower (median reduction less than ~15%) and there are more pronounced differences between experiments.

These results and the low reduction in NEE and FAPAR RMSDs following the assimilation atmospheric CO_2 data described above highlight the predominance of the correction of the trend in atmospheric CO_2 time series through the fitting of the carbon pool parameters, over the tuning of the other model parameters related to photosynthesis and phenology (see Figure 3). The 2-step approach permits to partially overcome that limitation, with the improvement of the mean seasonal cycle for the three data streams (Figure 2c).

Supprimé[Cédric Bacour]: Again, t

Mis en forme[cbacour]: Indice

3.1.3 Specific improvements at CO_2 stations

Figure 3 further analyzes the impact of each assimilation experiment on the fit to the observed atmospheric CO_2 concentrations in terms of the bias in the long-term trend (2000-2009) and fit to the mean seasonal cycle over the same period (i.e., bias in seasonal amplitude and length of the carbon uptake period - see Supplementary text S2 and Figure S1 for representative comparisons of observed

vs modeled time series of atmospheric CO_2 concentrations and their associated trend estimation).

For the trend analysis (Figure 3a), only experiments where atmospheric CO_2 measurements are assimilated are considered.

With the default (prior) parameter values, the fluxes simulated by ORCHIDEE and transported by LMD_Z overestimate the (trend) by about 1 ppm.yr^{-1}. When assimilating atmospheric CO_2 data, most of the parameter correction aims at reducing this bias. This is mostly achieved by tuning the regional K_{soilC_reg} parameters: the net land carbon sink is increased globally in order to match the observed trend at most stations (reducing the bias from around 1 ppm.yr^{-1} to 0.1 ppm.yr^{-1}). Compared to the improvement in the bias in the trend, the improvements (reduction in bias) in the amplitude of the CO_2 seasonal cycle and in the length of the carbon uptake period (CUP) (Figures 3b and c) are marginal. Note that our joint DA experiments lead to significantly lower trend biases compared to the stepwise approach.

For the amplitude of CO_2 concentrations, the joint assimilations including CO_2 data lead to lower improvements on average compared to any single data stream assimilation experiment. Interestingly, the highest improvements in CO_2 amplitude are achieved when flux data are assimilated (F or F+VI), which reveals that the constraint on photosynthesis and respiration provided by FLUXNET measurements is consistent with the amplitude of the seasonal atmospheric CO_2 cycle and within the ORCHIDEE-LMDz model (as already pointed out in Kuppel et al. (2014)). Surprisingly, the use of satellite vegetation indices (VI) leads to a slightly lower residual amplitude bias than when atmospheric CO_2 data are assimilated, albeit a lower number of optimized parameters. For the length of the CUP, the relative model correction appears small for almost all experiments and is lower than what is achieved for the trend and amplitude. Some degradation (increased model-data bias) is even obtained for the cases F and F+CO2. This may be attributed to some inconsistency in the phasing of the CUP derived from the FLUXNET stations and from the atmospheric stations (given differences in the spatial and temporal scale constraints brought each data stream). Among the single data stream assimilations, the highest improvement is obtained for VI where the optimisation of the phenological parameters was the only improvement allowed for tuning the model. For the joint assimilations, those combining the three data streams provide the best performance and perform better than the stepwise approach.

Among the joint assimilations with three data streams, the 2-step approach results in the largest reduction in amplitude and CUP bias, but, on the other hand, the larger trend bias.

Supprimé[Cédric Bacour]: simulated

Supprimé[Cédric Bacour]: lead

Supprimé[Cédric Bacour]: with

Supprimé[Cédric Bacour]: to

Supprimé[Cédric Bacour]: s

Supprimé[Cédric Bacour]: CUP

Supprimé[Cédric Bacour]: , which is probably due to the longer period of the atmospheric CO

Mis en forme[Cédric Bacour]: Pas Surlignage

Mis en forme[Cédric Bacour]: Pas Surlignage

Supprimé[Cédric Bacour]: carbon uptake period (

Supprimé[Cédric Bacour]:)

Supprimé[cbacour]: deduced

Supprimé[Cédric Bacour]:

3.2 Impact of the assimilations on regional to global land C fluxes and errors

Figure 4 now compares the carbon fluxes (NEE and GPP) at the global scale and for three large regions (northern and southern extra-tropics, and tropics) using hindcast simulations based on the different optimisations.

NEE is close to equilibrium by construction in the prior model (about -0.3 GtC.yr^{-1} globally). Note first that experiments excluding CO_2 data produce land carbon fluxes (from -10 (F+VI) to +6 (VI) GtC.yr^{-1}, not shown in Figure 3) that are not compatible with our understanding of the land C fluxes. For all experiments including atmospheric CO_2 data, the assimilations lead to much more negative NEE (increased land carbon sink) compared to the prior for nearly all regions: the optimized carbon sinks are about -2.4 GtC.yr^{-1} at the global scale, similar to the stepwise approach (see Supplementary Text S6 for detailed results for each assimilation experiment). Therefore, our joint assimilation with atmospheric CO_2 data results in a land C sink that is in the range of independent TBM estimates of the global net carbon budget (over the same period, the Global Carbon Project reports a global land sink of -2.9 GtC.yr^{-1} ± 0.8 standard deviation (see Table 5 of Friedlingstein et al., 2020). Note that we have imposed (see method in §2.1.2) a net emission from land use change (i.e. deforestation) of +1.1 GtC.yr^{-1} (2000-2009) which is slightly lower than that reported in Friedlingstein et al. (2020) from the TBMs (1.6±0.5 GtC.y^{r-1}) or the Bookkeeping methods (1.4±0.7 GtC.yr^{-1}), hence our lower terrestrial carbon sink.

These similar posterior global scale budgets however hide large regional contrasts. While the three joint assimilation experiments F+CO2, VI+CO2, and F+VI+CO2, lead to similar NEE budgets across regions (with magnitudes comparable to the stepwise assimilation set-up), the CO2 and F+VI+CO2-2steps experiments result in distinctly different estimates. In the northern extra-tropics, the CO2 assimilation results in the largest C sinks (numbers provided in Supplementary Text S6) while the F+VI+CO2-2steps assimilation leads to the lowest C sink. The reverse is obtained for the Tropics.

With a global scale budget of 171 GtC.yr^{-1} for GPP, the prior ORCHIDEE model is on the high range of recent estimates of the global GPP, as synthesized in Anav et al. (2015), the mean value of which being around 140 GtC.yr^{-1}. Depending on the data assimilated in this study, the posterior GPP ranges from 147 GtC.yr^{-1} (F+VI) to 170 GtC.yr^{-1} (VI+CO2) at the global scale. The largest differences with the prior are obtained for the experiments involving flux and satellite data (alone or the two combined). This is directly linked to large corrections in photosynthesis parameters for these experiments (see §3.3). In comparison, the assimilations involving atmospheric CO_2 concentrations data are more conservative with respect to GPP. Assimilating atmospheric CO_2 data alone lessens the GPP reduction by a factor of about three compared to assimilations with F and VI data, and the corrections for the joint assimilations using CO_2 data is even lower (cf Supplementary Text S6 for details).

Supprimé[Cédric Bacour]: These were however obtained without a new spin-up nor any transient simulations like it is

Supprimé[Cédric Bacour]: . For these experiments that

Supprimé[Cédric Bacour]: , which is -1.7GtC.yr^{-1}

Supprimé[Cédric Bacour]: 1

Supprimé[Cédric Bacour]: Note that the lower terrestrial

Supprimé[Cédric Bacour]: significant

Supprimé[Cédric Bacour]: , with a magnitude that match

Supprimé[Cédric Bacour]: Partitioning the land carbon

Supprimé[Cédric Bacour]:

Supprimé[Cédric Bacour]:

Supprimé[Cédric Bacour]: scientific question, in particula

Supprimé[Cédric Bacour]: , possibly due to CO

Mis en forme[Cédric Bacour]: Pas Surlignage

Supprimé[Cédric Bacour]:

Mis en forme[Cédric Bacour]: Pas Surlignage

Supprimé[Cédric Bacour]:

Supprimé[Cédric Bacour]: stepw

Supprimé[Cédric Bacour]: and the stepwise

Supprimé[Cédric Bacour]: lead to an approximately equa

Supprimé[Cédric Bacour]:

Mis en forme[Cédric Bacour]: Motif: 0(Couleur personna

Supprimé[cbacour]: (

Supprimé[Cédric Bacour]: note that we include all

Supprimé[cbacour]: greatest

By propagating the error on the parameters (see § 3.3) in the observation space (see Eq. 9), we calculated the uncertainty in NEE and GPP fluxes caused by parameter uncertainty for the prior and optimized models. The error statistics, initially calculated at monthly/grid scale resolutions, were aggregated over the same regions as above, fully accounting for the spatio-temporal correlations between grid cells (Figure 5).

At the global scale, the prior error standard deviation for NEE (4.7 $GtC.yr^{-1}$) is high compared to the typical uncertainty associated to TBMs (about 0.5 $GtC.yr^{-1}$, Friedlingstein et al. (2020)) or to atmospheric inversions (estimated uncertainty ~0.4 $GtC.yr^{-1}$ in Peylin et al.(2013)). This is a consequence of neglecting negative error correlations between them (as done in nearly all C cycle DA studies). Given this high prior uncertainty, the posterior error for NEE and GPP are significantly reduced, as expected. Because of the strong dependence of the posterior errors on the optimisation set-up and the fact we do not consider the error of the model, we should only compare the relative error reduction between DA experiments. Noteworthy, the posterior errors in global NEE obtained for the experiments CO2 and VI+CO2 are about 15 times lower than the posterior errors resulting from the other data combinations (and three orders of magnitude lower than the prior error). This is due both i) to the need for the DA system to correct the large *a priori* mismatch of the atmospheric CO_2 growth rate and ii) to the lower number of optimized parameters in these configurations (Table 2: about 60% more parameters being optimized in F+VI+CO2 than in CO2 or VI+CO2). The joint assimilations result in higher posterior errors on NEE, while they usually lead to the lower posterior errors on GPP. For GPP, the lowest posterior errors are found for the experiments combining F and CO2 data, while experiments F, CO2 and VI+CO2 lead to larger posterior errors . This is due to the fact that i) F and CO2 data provide a stronger constraint on the annual mean photosynthesis than VI data and that ii) F and CO2 data provide cross constraints on photosynthesis. Experiment VI, in which about ten times fewer parameters are optimized and targeting primarily the timing of phenology, results in the highest posterior GPP errors (although still a reduction from the prior).

Finally, one can observe that the posterior errors are higher in the tropics for both NEE and GPP (and the reduction compared to the prior error is lower), which is even more prominent in the experiments using *in situ* flux data alone or with satellite data, a direct consequence of the lower data availability (eddy-covariance measurements) to constrain the model parameters for tropical PFTs.

3.3 Parameter estimates and associated uncertainties

Figure 6 shows the impacts of the different assimilation experiments on a subset of the retrieved parameter values and their associated uncertainties (the remaining parameters are shown in Figure S2).

While the stepwise study showed only few changes in the parameter estimates between the sequential steps (and hence as a function of the data stream from which the parameters were constrained) (Peylin et al., 2016), our results show a large variability between the assimilation experiments. For most parameters, the highest departures from the prior values are obtained for single-data stream assimilations. Higher changes are obtained for flux or satellite data as compared to the estimates retrieved with atmospheric CO_2 data alone which remain closer to the prior values. This reflects the lower constraint brought by the CO2 assimilation experiment on photosynthesis and phenology related processes, as already pointed out in §3.1.2. This is largely due to the correction of the trend bias via a few respiration related parameters, which prevails over the improvement of the other photosynthesis and phenology parameters.

The joint assimilations usually result in a lower departure from the background. For the parameters constrained by two data streams, the optimized values generally fall in between those retrieved when these data streams are assimilated alone. This feature shows how the system tries to find a compromise solution and illustrates potential overfitting with only one data stream. The values optimized in the three experiments involving atmospheric CO_2 data show little variability for all parameters, except in F+VI+CO2-2steps where the tuning of the multiplicative parameter of regional soil carbon pools K_{soilC_reg} is decoupled from the optimization of the other photosynthesis and phenological parameters. The decrease of K_{soilC_reg} parameters from the prior value is very small in all experiments, although these parameters are responsible for most of the correction of the atmospheric CO_2 trend. This highlights the challenge of optimizing soil C disequilibrium with our approach based on a model spin-up followed by only a short transient period. The smallest K_{soilC_reg} changes are obtained for the 2-step approach. Note that in this approach, *Q10* is also estimated in the first step; the corresponding estimate is similar to the value retrieved in the second step (which is displayed in Figure 3), below 0.5% difference, and consistent with the estimates of the other joint assimilation experiments. For some parameters/PFTs, the direction of the departure with respect to the prior value (increase or decrease) may differ depending on the data stream assimilated (as detailed in S5).

At the first order, the estimated parameter uncertainties decrease with the number of observations assimilated, as expected from Equation 4, and given that the observations are treated as independent data. However, given that the estimated parameter errors strongly depend on the set-up of **B** and **R** matrices and that we did not use error correlations in these matrices, we should only

Supprimé[cbacour]: 1

Supprimé[Cédric Bacour]: The estimates are compared to the posterior parameters from the stepwise approach used in Peylin et al. (2016).

Supprimé[Cédric Bacour]: (either between experiments considering a single data stream or between single- vs joint-assimilations)

Supprimé[Cédric Bacour]: (based on two or three data streams)

Supprimé[Cédric Bacour]: without

Supprimé[Cédric Bacour]: run

focus on the relative error reduction between experiments. The uncertainty reduction achieved through the assimilation of atmospheric CO_2 data is usually lower than when flux and satellite data are assimilated alone, and typically vary between 10% and 60% for most photosynthetic and phenological parameters. Most often, the joint assimilations involving two data streams result in an uncertainty reduction higher or of the same order than that achieved in the single-data assimilations. The joint assimilation combining the three data streams generally results in the highest uncertainty reduction, with values typically between 60% and 90%. The values are much higher than those inferred from the stepwise approach, which are more on the order of the uncertainty reduction obtained in the CO2 assimilation experiment.

Supprimé[Cédric Bacour]: (at the last step where three years of atmospheric CO_2 data were assimilated)

3.4 Relative constraints brought by the different datasets

We now quantify the impact of each of the three data streams on the analysis using the global average observation influence (quantified by OI) and information content (DFS) metrics defined in § 2.4.4. We recall that OI (i.e. trace of **S** normalized by the number of observations) gauges the average influence that each single observation has on the analysis, while the relative DFS measures the overall weight of one data stream in the optimization (the difference between OI and DFS is due to the number of observations assimilated, Cardinali et al. (2014)). OI and DFS are determined for the joint assimilation experiments combining the three data streams.

Supprimé[Cédric Bacour]:

Because of the very large number of observations (above 300,000) involved in the assimilation, only the diagonal elements of the influence matrix (Eq. 10) can be calculated. The trace of **S** measures the equivalent number of parameters and is equal to 132. Such a value, lower than the number of parameters (182), indicates that the optimized parameters may not be fully independent (although parameter error correlations have been ignored in our **B** matrix) as already reported in Kuppel et al. (2012), or that some are not constrained during the optimisation process (as for instance LAI_{MAX} which estimates remains at its *a priori* value for some PFTs, Figure S2).

Supprimé[cbacour]: 1

The values of OI are provided in Table 4 for flux, NDVI and atmospheric CO_2 data. With about the same number of observations considered (Table 2, last column), one *in situ* flux measurement has about 10 times more weight than one NDVI observation. This is a consequence of the larger number of parameters constrained by flux measurements than by NDVI data in our set-up. The highest influence is found for atmospheric CO_2 data, the relative weight of one atmospheric CO_2 measurement being 4 times greater than that of one flux observation, albeit the much lower number of data assimilated. Again, this is a consequence of the strong weight of the mismatch between the *a*

Supprimé[Cédric Bacour]: T

priori simulated and the observed atmospheric CO_2 trend, which is drastically reduced through the optimisation.

However, the smaller number of atmospheric CO_2 data assimilated, compared to flux and NDVI datasets, reduces the overall constraint on the analysis provided by atmospheric CO_2 data, as gauged by its relative DFS. Hence, our optimization is mainly controlled by flux data which have an overall contribution of about 75%, that is about 5 times larger than the constraint brought by atmospheric CO_2 data and 7 times larger than that of satellite NDVI. Differences between F+VI+CO2 and F+VI+CO2-2steps are relatively small for both OI and DFS but show a slightly lower weight of atmospheric CO_2 data for the 2 steps experiment. A complementary analysis in which the influence of each PFT and each atmospheric station is differentiated is provided in Supplementary Text S7.

4 Discussion

4.1 Benefits of simultaneous assimilations

Joint/simultaneous assimilations are more complex to implement compared to stepwise/sequential assimilations. In principle a stepwise approach could lead to similar results than a simultaneous approach, if the posterior parameter error covariance matrix could be fully characterized at each assimilation step and further propagated as prior information in the next step. However, given that this is difficult in practice, and because of model non-linearities and equifinal solutions, stepwise/joint approaches lead to different optimized models (Kaminski et al., 2012; MacBean et al. 2016). With a joint assimilation, biases and incompatibilities between data streams may impact more directly a larger set of parameters than in a stepwise assimilation. The characterization of the prior observation errors also becomes more critical as they condition the relative weight of the observations in the misfit function to minimize and their influence on the solution (analysis). Here, we designed several tests beforehand to refine the configuration of the framework for the simultaneous assimilations. Relying on consistency metrics of Desroziers et al. (2005), we improved the prior error statistics on the model parameters and checked that they were consistent with both the prior model-data mismatch and the observations errors for the different data streams. In spite of the limitation of their application to non-linear models like ORCHIDEE, their implementation has proved to be useful and has led to an improved consistency of the optimized models at regional and global scales.

Supprimé[Cédric Bacour]: (over 10 years)
Supprimé[Cédric Bacour]: The same analysis was perfor
Supprimé[Cédric Bacour]: For satellite NDVI data howev
Supprimé[Cédric Bacour]:
Supprimé[Cédric Bacour]: **For atmospheric CO_2 data, the**
Supprimé[Cédric Bacour]: **Summary and outlook**
Supprimé[Cédric Bacour]: By assimilating separately or
Supprimé[Cédric Bacour]: The successive model evaluati
Mis en forme[Cédric Bacour]: Motif: 0(Couleur personna
Supprimé[Cédric Bacour]:
Mis en forme[Cédric Bacour]: Motif: 0(Couleur personna
Supprimé[Cédric Bacour]: Our analyses focussed not onl
Mis en forme[Cédric Bacour]: Motif: 0(Couleur personna
Supprimé[Cédric Bacour]: also
Mis en forme[Cédric Bacour]: Motif: 0(Couleur personna
Supprimé[Cédric Bacour]: highlighted some challenges ir
Mis en forme[Cédric Bacour]: Motif: 0(Couleur personna
Supprimé[Cédric Bacour]: here related to the
Mis en forme[Cédric Bacour]: Motif: 0(Couleur personna
Supprimé[Cédric Bacour]: in particular the
Mis en forme[Cédric Bacour]: Motif: 0(Couleur personna
Supprimé[Cédric Bacour]:
Mis en forme[Cédric Bacour]: Motif: 0(Couleur personna
Supprimé[Cédric Bacour]: joint
Supprimé[cbacour]:
Supprimé[Cédric Bacour]: not feasible
Supprimé[cbacour]:
Supprimé[cbacour]: also
Supprimé[cbacour]: Hence, w
Supprimé[cbacour]: , r
Supprimé[cbacour]: on parameter and observation error
Supprimé[cbacour]: to assign the error statistics on prior
Supprimé[cbacour]:

Single data stream assimilations usually lead to the best model - data fit for the assimilated data stream, as compared to joint assimilations. However, most often these single data stream assimilations also produce degraded results with respect to the data that were not assimilated. This reveals potential overfitting issues with a higher variability of the optimized parameter values than in the joint assimilations. Overfitting is a key issue for DA studies which can be partly alleviated when combining different data streams within a consistent framework: because they bring different information on the model processes, they contribute to better circumscribing a set of model parameters. Among the several assimilation experiments considered, those where several data were assimilated simultaneously were those in which there was always an improvement in optimized variables (i.e. no deterioration in model-data fit). The joint assimilations resulted in a reduced variability in parameter estimates and in optimized NEE and GPP.

4.2 Realism of the regional to global-scale C fluxes

The overarching objective of the study was more about assessing how to make the best of a synergistic exploitation of different data streams within a consistent assimilation framework rather than achieving an up-to-date re-analysis of the global carbon fluxes. Especially since we focused on a limited dataset both in terms of temporal coverage (no atmospheric CO_2 data nor satellite data after 2010, no *in situ* flux data beyond 2007) and of informational constraint. Indeed, we did not assess the potential of other data that can bring relevant (and possibly more direct) additional constraints on the dynamics of terrestrial carbon stocks and fluxes, such as aboveground biomass (Thum et al., 2017) or Solar Induced-Fluorescence (Bacour et al., 2019) which have already been investigated with ORCHIDAS, and with an updated version of the ORCHIDEE model. The expansion of the assimilated datasets to provide the most up-to-date constraint on modeled carbon fluxes will be the subject of future work.

In spite of these limitations, we saw that the regional/global estimated NEE and GPP budgets are realistic and in agreement with independent estimates. There are still important differences in the model predictions for the different assimilation experiments (and we have not attempted to identify what was the most reliable optimized model, which would require the use of an ensemble of independent data, an effort beyond the scope of this paper). Still, our optimised simulations allow a more in depth exploration of the partitioning of the land carbon budget between the northern extra-tropics and the tropics. From the global carbon budget, a discrepancy exists between the partition estimated by the atmospheric CO_2 inversions and by the terrestrial biosphere models (Kondo et al., 2020). Atmospheric inversions estimate a larger sink over the northern extra-tropics than TBMs

Supprimé[cbacour]: pieces to
Supprimé[cbacour]: resulting in the least model degradat
Supprimé[cbacour]: J
Supprimé[cbacour]: regularized the system and
Supprimé[Cédric Bacour]: In order to investigate the
Supprimé[Cédric Bacour]: : In addition, we acknowledge
Supprimé[cbacour]: content
Supprimé[Cédric Bacour]: that
Supprimé[Cédric Bacour]: information
Supprimé[Cédric Bacour]: and stocks
Supprimé[cbacour]:
Supprimé[cbacour]:
Supprimé[Cédric Bacour]:
Supprimé[Cédric Bacour]:
Supprimé[cbacour]:
Supprimé[Cédric Bacour]: However,
Supprimé[Cédric Bacour]: ;
Supprimé[cbacour]:
Supprimé[cbacour]:
Supprimé[Cédric Bacour]: but t
Supprimé[cbacour]:
Supprimé[Cédric Bacour]: . We
Supprimé[Cédric Bacour]: (
Supprimé[cbacour]: Let look analyze in more details the
Supprimé[Cédric Bacour]: P
Supprimé[cbacour]:
Supprimé[cbacour]:
Supprimé[cbacour]:
Supprimé[cbacour]: that are inferred among the several
Supprimé[Cédric Bacour]: is a key scientific question, in
Supprimé[cbacour]: .

(around 1.8 GtgC.yr^{-1} versus 1.0 GtC.yr^{-1} for the period 2010-2020), although with large variations between TBMs (Friedlingstein et al., 2020, Figure 8). Conversely, TBMs estimate a larger C sink over the tropics (Ahlström et al., 2015; Sitch et al., 2015), possibly due to strong CO_2 fertilization effects in TBMs (Schimel et al., 2015), than the inversions, which estimate an approximately net neutral C sink (Peiro et al., 2022). The F+VI+CO2-2steps assimilations follow the typical partitioning pattern of TBMs' behavior, with a stronger C sink in the tropics than in the northern hemisphere (Figure 4). In contrast, all other multiple data stream experiments with CO2 included (F+CO2, VI+CO2 and F+VI+CO2) and the stepwise lead to an approximately equal C sink in the northern hemisphere and tropics (thus unlike the general pattern for TBMs, and more in line with atmospheric inversions); And on the other hand, the CO2 experiment leads to a similar regional partitioning as the atmospheric inversions. For the F+VI+CO2-2steps experiment, the tropical sink is almost doubled as compared to the other simultaneous assimilation experiments in spite of a slightly reduced GPP.

4.3 Caveats and perspectives concerning the initialisation of the soil carbon pools

We showed that reaching the global terrestrial carbon sink was mostly achieved by correcting the initial soil carbon reservoirs in the ORCHIDEE model. Their tuning enables the correction of the biased trend between atmospheric CO_2 time series measurements at stations and the prior ORCHIDEE-LMDz model. The impact of this biased trend on the optimization performance was highlighted by the quantification of the influence for the three data streams on the optimization, with atmospheric CO_2 data having the largest average observation influence on the solution. A consequence of correcting the biased trend is that the model improvement with respect to other processes (photosynthesis, phenology) is hindered.

From a more general perspective, the detrimental consequences of model-data biases become even more important when assimilating multiple observational constraints because of their interconnected contribution to the model calibration. It should be noted that the impact of systematic model-data errors is not inherent to our minimization approach (gradient-based) and has also been highlighted using random search approaches (Brynjarsdóttir and O'Hagan, 2014; Cameron et al., 2021). Thus, the importance of accounting for bias correction approaches into data assimilation schemes (Dee, 2005; Trémolet, 2006; Kumar et al., 2012) becomes increasingly important as the complexity of models and the number of observational constraints increase.

We attempted here to overcome this by setting up a 2-step assimilation process where the trend correction is mostly achieved in the first step by tuning the regional parameters controlling the soil carbon pools. In doing so, the 2-step approach optimizes the constraint brought by *in situ* and satellite data (in the second step) in the joint assimilation process. Therefore, the 2-step results in

Supprimé[Cédric Bacour]: stepwise and

Supprimé[cbacour]: On the opposite

Supprimé[cbacour]: the three two or more

Supprimé[cbacour]: .

Supprimé[cbacour]: In contrast, the CO2 experiment leads to a similar regional partitioning as the atmospheric inversions.

Supprimé[cbacour]: The correction of the CO_2 trend in the first step of the 2-step approach, with the optimisation of the soil disequilibrium (K_{soilC_reg} parameters), tends to favor a …

Mis en forme[Cédric Bacour]: Motif: 0(Couleur personnalisée (RVB(255,153,0)))

Mis en forme[Cédric Bacour]: Motif: 0(Couleur personnalisée (RVB(255,153,0)))

Mis en forme[Cédric Bacour]: Motif: 0(Couleur personnalisée (RVB(255,153,0)))

Mis en forme[Cédric Bacour]: Motif: 0(Couleur personnalisée (RVB(255,153,0)))

Supprimé[Cédric Bacour]: Interestingly, we noticed that the multi-data stream assimilations including CO_2 data (except the 2-step case) lead to a partition of the terrestrial C sink …

Supprimé[cbacour]:

Supprimé[cbacour]: this

Supprimé[cbacour]: bias

Supprimé[cbacour]: bias

Supprimé[cbacour]: greatest

Supprimé[cbacour]:

Supprimé[cbacour]: A consequence of correcting the trend bias is that the model improvement with respect to other processes (photosynthesis, phenology) is hindered.

Supprimé[cbacour]:

enhanced model-data consistencies compared to a standard simultaneous assimilation (as observed in Figure 2 and Figure 3) with a caveat regarding atmospheric CO_2 data (the improved fit is mostly with the detrended atmospheric CO_2 data but not the raw data) and the distribution of the land C sink (we saw above that this experiment tends to favor a tropical C sink) . We acknowledge the fact that this way of doing is not optimal and requires further investigation. Going beyond the steady state assumption following model spin-up has been discussed already (Carvalhais et al., (2010); MacBean et al., 2022), as steady state results in biased estimates of soil carbon reservoirs (Exbrayat et al., 2014). Extending the period for the transient simulations following spin-up, like it is done in the TRENDY experiment (Sitch et al., 2015), would have led to more realistic soil C imbalance and increased the consistency of the modelled atmospheric data with the measurements. Improving the representation of soil carbon stock trajectories in TBMs is pivotal to predicting NEE in regional to global assessments of the capacity of the terrestrial ecosystems to absorb or not atmospheric CO_2. We used here atmospheric CO_2 data to optimize a scalar that accounts for the soil C disequilibrium. The optimization of scaling factors of soil carbon pools is a handy alternative to the optimization of the parameters controlling the turnover times and soil carbon input of the ORCHIDEE soil C model. This would require that the spin-up (over at least one thousand years) and transient simulations are included in the minimization process at each iteration; the prohibitive calculation times for performing this type of optimisation precludes us doing this for now. Exploiting in TBMs databases more directly related to regional soil carbon contents (such as the Harmonized World Soil Database (HWSD) (FAO/IIASA/ISRIC/ISSCAS/JRC, 2012), the International Soil Carbon Network, Nave et al. (2016), or the global soil respiration database, Jian et al. (2021)) is not straightforward because of the errors associated these datasets (Todd-Brown et al., 2013), and inconsistencies between the estimated quantities and the model state variables and underlying processes (as for instance the depth of the soil carbon) . In any case, what is sorely needed is data that track changes in C stocks over long time periods. Still, it is of primary importance for the science community to endeavor to bridge the gap between state-of-the art estimates of soil carbon stocks and the quantities that TBMs simulate over the historical period.

5 Conclusion

By assimilating simultaneously or separately up to three independent carbon-cycle related data streams (*in situ* measurements of net carbon and latent heat fluxes, satellite derived NDVI data, and measurements of atmospheric CO_2 concentration at surface stations) within the ORCHIDEE global model (and an offline transport model based on pre-calculated transport fields with LMDz), we have been able to analyze their compatibility, complementarity, and usefulness, in the frame of a global-

Supprimé[Cédric Bacour]: :
Supprimé[cbacour]: already
Supprimé[cbacour]: s
Mis en forme[cbacour]: Indice
Supprimé[Cédric Bacour]:
Supprimé[cbacour]:
Supprimé[Cédric Bacour]: But most importantly, it highli…
Supprimé[cbacour]:
Supprimé[cbacour]:
Supprimé[Cédric Bacour]: constrain
Supprimé[cbacour]:
Supprimé[cbacour]: m but they convey C cycle related…
Supprimé[cbacour]: as
Supprimé[cbacour]: plus
Supprimé[cbacour]: the
Supprimé[cbacour]: the
Supprimé[cbacour]: to be
Supprimé[cbacour]: (hence an update
Supprimé[cbacour]:)
Supprimé[cbacour]: T
Supprimé[cbacour]: so
Supprimé[cbacour]:…
Supprimé[Cédric Bacour]: by TBMs
Supprimé[cbacour]: ing
Supprimé[cbacour]: what
Supprimé[cbacour]:…
Supprimé[cbacour]: or simultaneously
Mis en forme[cbacour]: Police: Italique
Mis en forme[cbacour]: Indice

scale carbon data assimilation system. To do so, the study relied on different metrics to set-up and interpret the assimilation performances. The approach as well as the explored metrics are general enough to benefit to a broader set of data assimilation applications, supporting guidance for setting up such a C cycle DA framework and for better use of the data to be assimilated.

We investigated how the different combinations of data streams constrain the parameters of the ORCHIDEE land surface model, and by consequence the simulated historical spatial and temporal distribution of the net and gross carbon fluxes (NEE and GPP), as well as FAPAR and atmospheric CO_2 concentrations. We quantified how the combination of these data-streams (two by two or alltogether) impacts the reliability of the model predictions. Although it leads to lower fitting performances with respect to the assimilation of any individual dataset (because the optimization seeks for a trade-off solution between all data-streams) the simultaneous assimilation of the three data-streams is found to be the most consistent approach. In particular, it avoids model overfitting which can degrade the model predictions with respect to data-streams not assimilated. The successive model evaluations performed after the assimilation highlighted challenges in handling model-data bias in Bayesian optimisation frameworks.

In this study, we focused on biases associated to the initialisation of the soil carbon pools in our set-up (the fact that they are out of equilibrium because of all historical land cover change and land mangement impacts. A carefull spin-up including a transient simulation to account for the impact of all past disturbances (climate, land cover, land management) is mandatory but likely not sufficient (due to uncertainties in the historical evolution of these drivers) to achieve accurate simulation of the space-time distribution of the global land C sink. Next steps should focus on including part of the spin-up (i.e. such as the transient simulation) in the assimilation procedure possibly in conjunction with initial C pool optimisation.

Terrestrial ecosystem modelers are anticipating the many novel types of observations that are being made available for model evaluation and assimilation. As a result, and in parallel to the growing complexity of TBMs incorporating new biogeo- physical processes related to the carbon and water cycles, new observation operators are being developed to be able to make use of this new wealth of data. With these new perspectives ahead, the global land surface modeling community should investigate more deeply some of the issues highlighted in this study and linked to multiple data streams assimilation, initial model state optimisation and/or the inclusion of the spin up in the DA system, etc., in order to achieve significant reduction in land surface model projection uncertainties.

Code availability

Supprimé[cbacour]: We hope that the metrics explored can

Supprimé[cbacour]: the

Supprimé[cbacour]:

Mis en forme[cbacour]: Indice

Supprimé[cbacour]: We saw that the data-stream combination matters and

Supprimé[cbacour]: the whole data and with the model

Supprimé[cbacour]:
It is here related to incorrect initialisation of the soil our set-up. This finding pleads for more consistent approaches to do the task in TBMs, so as to ultimately improve the accuracy in their simulation of the space-time distribution of the global land carbon sink.

Mis en forme[cbacour]: Gauche, Bordure: Haut: (Pas de bordure), Bas: (Pas de bordure), Gauche: (Pas de bordure), Droite: (Pas de bordure), Entre: (Pas de bordure)

Supprimé[cbacour]: g

Supprimé[Cédric Bacour]: We hope that the metrics explored in this study can benefit a broader set of data assimilation applications, supporting guidance for setting up the framework and for better use of the data to be assimilated.

The ORCHIDEE model code is open source (http://forge.ipsl.jussieu.fr/orchidee) and the associated documentation can be found at https://forge.ipsl.jussieu.fr/orchidee/wiki/Documentation. The ORCHIDAS data assimilation scheme (in Python) is available through a dedicated web site (https ://orchi das.lsce.ipsl.fr/). Information about the LMDz model, source code and contact is provided at https://lmdz.lmd.jussieu.fr/le-projet-lmdz-en-bref-en.

Data availability

This work used eddy covariance data acquired by the FLUXNET community (https://fluxnet.org/data/la-thuile-dataset/). The NDVI data are derived from the MODIS MOD09CMG collection 5 daily global reflectance products (‘https://ladsweb.modaps.eosdis.nasa.gov/missions-and-measurements/products/MOD09CMG). The surface atmospheric CO_2 concentration data uses measurements from The NOAA Earth System Laboratory (ESRL) archive (ftp://ftp.cmdl.noaa.gov/ccg/co2/), the CarboEurope IP project (http://ceatmosphere.lsce.ipsl.fr/database/index_database.html), and the World Data Centre for Greenhouse Gases of the World Meteorological Organization Global Atmospheric Watch Programme (http://gaw.kishou.go.jp).

Author contributions

CB, NM, PP and FC conceived the research. CB developed the data assimilation system with contribution from FC (coupling with LMDz) and SL (parallelisation and post-processing). PP developed the offline transport (precomputed Jacobian matrix of LMDz) with contribution from SL. CB conducted the analysis, with contributions from NM and SL for spin-up ORCHIDEE simulations. PP, FC, and EK, provided the ancillary input fluxes for the global-scale simulations. EK and CB contributed to the development of the tangent linear version of the ORCHIDEE model. CB conceived and wrote the original draft with NM, PP, and FC. All co-authors reviewed the paper.

Acknowledgements

This work has been supported by the CARBONES project, within the EU’s 7th Framework Program for Research and Development. The authors are very grateful to LSCE's IT staff for their support and for the computing resources, as well as to the ORCHIDEE Project Team for developing and maintaining the ORCHIDEE code.

References

Ahlström, A., Raupach, M. R., Schurgers, G., Smith, B., Arneth, A., Jung, M., Reichstein, M., Canadell, J. G., Friedlingstein, P., and Jain, A. K.: The dominant role of semi-arid ecosystems in the trend and variability of the land CO2 sink, 348, 895–899, 2015.

Anderson, J., Hoar, T., Raeder, K., Liu, H., Collins, N., Torn, R., & Avellano, A. (2009). The data assimilation research testbed: A community facility. Bulletin of the American Meteorological Society, 90(9), 1283-1296.

Arora, V. K., Katavouta, A., Williams, R. G., Jones, C. D., Brovkin, V., Friedlingstein, P., Schwinger, J., Bopp, L., Boucher, O., and Cadule, P.: Carbon–concentration and carbon–climate feedbacks in CMIP6 models and their comparison to CMIP5 models, 17, 4173–4222, 2020.

Bacour, C., Peylin, P., MacBean, N., Rayner, P. J., Delage, F., Chevallier, F., Weiss, M., Demarty, J., Santaren, D., and Baret, F.: Joint assimilation of eddy covariance flux measurements and FAPAR products over temperate forests within a process-oriented biosphere model, 120, 1839–1857, 2015.

Bacour, C., Maignan, F., Peylin, P., Macbean, N., Bastrikov, V., Joiner, J., Köhler, P., Guanter, L., and Frankenberg, C.: Differences between OCO-2 and GOME-2 SIF products from a model-data fusion perspective, 124, 3143–3157, 2019.

Bastrikov, V., MacBean, N., Bacour, C., Santaren, D., Kuppel, S., and Peylin, P.: Land surface model parameter optimisation using in situ flux data: comparison of gradient-based versus random search algorithms (a case study using ORCHIDEE v1. 9.5. 2), 11, 4739–4754, 2018.

Botta, A., Viovy, N., Ciais, P., Friedlingstein, P., and Monfray, P.: A global prognostic scheme of leaf onset using satellite data, 6, 709–725, 2000.

Brynjarsdóttir, J., & O'Hagan, A. (2014). Learning about physical parameters: The importance of model discrepancy. Inverse problems, 30(11), 114007.

Byrd, R. H., Lu, P., Nocedal, J., and Zhu, C.: A limited memory algorithm for bound constrained optimization, 16, 1190–1208, 1995.

Supprimé[cbacour]:

Cameron, D., Hartig, F., Minnuno, F., Oberpriller, J., Reineking, B., Van Oijen, M., & Dietze, M. (2022). Issues in calibrating models with multiple unbalanced constraints: the significance of systematic model and data errors. Methods in Ecology and Evolution.

Cardinali, C., Pezzulli, S., and Andersson, E.: Influence-matrix diagnostic of a data assimilation system, 130, 2767–2786, 2004.

Carvalhais, N., Reichstein, M., Ciais, P., Collatz, G. J., Mahecha, M. D., Montagnani, L., Papale, D., Rambal, S., and Seixas, J.: Identification of vegetation and soil carbon pools out of equilibrium in a process model via eddy covariance and biometric constraints, 16, 2813–2829, 2010.

Cressot, C., Chevallier, F., Bousquet, P., Crevoisier, C., Dlugokencky, E. J., Fortems-Cheiney, A., Frankenberg, C., Parker, R., Pison, I., and Scheepmaker, R. A.: On the consistency between global and regional methane emissions inferred from SCIAMACHY, TANSO-FTS, IASI and surface measurements, 14, 577–592, 2014.

Crowell, S., Baker, D., Schuh, A., Basu, S., Jacobson, A. R., Chevallier, F., Liu, J., Deng, F., Feng, L., and McKain, K.: The 2015–2016 carbon cycle as seen from OCO-2 and the global in situ network, 19, 9797–9831, 2019.

Dee, D. P.: Bias and data assimilation, 131, 3323–3343, 2005.

Dee, D. P., Uppala, S. M., Simmons, A. J., Berrisford, P., Poli, P., Kobayashi, S., Andrae, U., Balmaseda, M. A., Balsamo, G., and Bauer, d P.: The ERA-Interim reanalysis: Configuration and performance of the data assimilation system, 137, 553–597, 2011.

Desroziers, G., Berre, L., Chapnik, B., and Poli, P.: Diagnosis of observation, background and analysis-error statistics in observation space, 131, 3385–3396, 2005.

Dietze, M. C., Lebauer, D. S., & Kooper, R. O. B. (2013). On improving the communication between models and data. Plant, Cell & Environment, 36(9), 1575-1585.

Dufresne, J.-L., Foujols, M.-A., Denvil, S., Caubel, A., Marti, O., Aumont, O., Balkanski, Y., Bekki, S., Bellenger, H., and Benshila, R.: Climate change projections using the IPSL-CM5 Earth System Model: from CMIP3 to CMIP5, 40, 2123–2165, 2013.

Exbrayat, J.-F., Pitman, A. J., and Abramowitz, G.: Response of microbial decomposition to spin-up explains CMIP5 soil carbon range until 2100, 7, 2683–2692, 2014.

Supprimé[cbacour]:

Forkel, M., Carvalhais, N., Schaphoff, S., Migliavacca, M., Thurner, M., and Thonicke, K.: Identifying environmental controls on vegetation greenness phenology through model–data integration, 11, 7025–7050, 2014.

Fox, A. M., Hoar, T. J., Anderson, J. L., Arellano, A. F., Smith, W. K., Litvak, M. E., MacBean, N., Schimel, D. S., and Moore, D. J.: Evaluation of a data assimilation system for land surface models using CLM4. 5, 10, 2471–2494, 2018.

Friedlingstein, P., O'Sullivan, M., Jones, M. W., Andrew, R. M., Hauck, J., Olsen, A., Peters, G. P., Peters, W., Pongratz, J., Sitch, S., Le Quéré, C., Canadell, J. G., Ciais, P., Jackson, R. B., Alin, S., Aragão, L. E. O. C., Arneth, A., Arora, V., Bates, N. R., Becker, M., Benoit-Cattin, A., Bittig, H. C., Bopp, L., Bultan, S., Chandra, N., Chevallier, F., Chini, L. P., Evans, W., Florentie, L., Forster, P. M., Gasser, T., Gehlen, M., Gilfillan, D., Gkritzalis, T., Gregor, L., Gruber, N., Harris, I., Hartung, K., Haverd, V., Houghton, R. A., Ilyina, T., Jain, A. K., Joetzjer, E., Kadono, K., Kato, E., Kitidis, V., Korsbakken, J. I., Landschützer, P., Lefèvre, N., Lenton, A., Lienert, S., Liu, Z., Lombardozzi, D., Marland, G., Metzl, N., Munro, D. R., Nabel, J. E. M. S., Nakaoka, S.-I., Niwa, Y., O'Brien, K., Ono, T., Palmer, P. I., Pierrot, D., Poulter, B., Resplandy, L., Robertson, E., Rödenbeck, C., Schwinger, J., Séférian, R., Skjelvan, I., Smith, A. J. P., Sutton, A. J., Tanhua, T., Tans, P. P., Tian, H., Tilbrook, B., van der Werf, G., Vuichard, N., Walker, A. P., Wanninkhof, R., Watson, A. J., Willis, D., Wiltshire, A. J., Yuan, W., Yue, X., and Zaehle, S.: Global Carbon Budget 2020, 12, 3269–3340, https://doi.org/10.5194/essd-12-3269-2020, 2020.

Giering, R., Kaminski, T., and Slawig, T.: Generating efficient derivative code with TAF: Adjoint and tangent linear Euler flow around an airfoil, 21, 1345–1355, 2005.

Groenendijk, M., Dolman, A. J., Van Der Molen, M. K., Leuning, R., Arneth, A., Delpierre, N., Gash, J. H. C., Lindroth, A., Richardson, A. D., and Verbeeck, H.: Assessing parameter variability in a photosynthesis model within and between plant functional types using global Fluxnet eddy covariance data, 151, 22–38, 2011.

Hourdin, F., Musat, I., Bony, S., Braconnot, P., Codron, F., Dufresne, J.-L., Fairhead, L., Filiberti, M.-A., Friedlingstein, P., and Grandpeix, J.-Y.: The LMDZ4 general circulation model: climate performance and sensitivity to parametrized physics with emphasis on tropical convection, 27, 787–813, 2006.

Jian, J., Vargas, R., Anderson-Teixeira, K., Stell, E., Herrmann, V., Horn, M., Kholod, N., Manzon, J., Marchesi, R., and Paredes, D.: A restructured and updated global soil respiration database (SRDB-V5), 13, 255–267, 2021.

Kaminski, T., Knorr, W., Rayner, P. J., and Heimann, M.: Assimilating atmospheric data into a terrestrial biosphere model: A case study of the seasonal cycle, 16, 14–1, 2002.

Kaminski, T., Knorr, W., Schürmann, G., Scholze, M., Rayner, P. J., Zaehle, S., Blessing, S., Dorigo, W., Gayler, V., and Giering, R.: The BETHY/JSBACH carbon cycle data assimilation system: Experiences and challenges, 118, 1414–1426, 2013.

Kato, T., Knorr, W., Scholze, M., Veenendaal, E., Kaminski, T., Kattge, J., and Gobron, N.: Simultaneous assimilation of satellite and eddy covariance data for improving terrestrial water and carbon simulations at a semi-arid woodland site in Botswana, 10, 789–802, 2013.

Keenan, T. F., Davidson, E. A., Munger, J. W., and Richardson, A. D.: Rate my data: quantifying the value of ecological data for the development of models of the terrestrial carbon cycle, 23, 273–286, 2013.

Knorr, W. and Heimann, M.: Impact of drought stress and other factors on seasonal land biosphere CO2 exchange studied through an atmospheric tracer transport model, 47, 471–489, https://doi.org/10.1034/j.1600-0889.47.issue4.7.x, 1995.

Knorr, W. and Kattge, J.: Inversion of terrestrial ecosystem model parameter values against eddy covariance measurements by Monte Carlo sampling, 11, 1333–1351, 2005.

Knorr, W., Kaminski, T., Scholze, M., Gobron, N., Pinty, B., Giering, R., and Mathieu, P.-P.: Carbon cycle data assimilation with a generic phenology model, 115, 2010.

Kondo, M., Patra, P. K., Sitch, S., Friedlingstein, P., Poulter, B., Chevallier, F., ... & Ziehn, T. (2020). State of the science in reconciling top-down and bottom-up approaches for terrestrial CO_2 budget. Global change biology, 26(3), 1068-1084.

Koffi, E. N., Rayner, P. J., Scholze, M., and Beer, C.: Atmospheric constraints on gross primary productivity and net ecosystem productivity: Results from a carbon-cycle data assimilation system, 26, 2012.

Krinner, G., Viovy, N., de Noblet-Ducoudré, N., Ogée, J., Polcher, J., Friedlingstein, P., Ciais, P., Sitch, S., and Prentice, I. C.: A dynamic global vegetation model for studies of the coupled atmosphere-biosphere system, 19, 2005.

Mis en forme[cbacour]: Indice

Supprimé[cbacour]:

Kumar, S. V., Reichle, R. H., Harrison, K. W., Peters-Lidard, C. D., Yatheendradas, S., & Santanello, J. A. (2012). A comparison of methods for a priori bias correction in soil moisture data assimilation. Water Resources Research, 48(3).

Kuppel, S., Peylin, P., Chevallier, F., Bacour, C., Maignan, F., and Richardson, A. D.: Constraining a global ecosystem model with multi-site eddy-covariance data, 9, 3757–3776, 2012.

Kuppel, S., Chevallier, F., and Peylin, P.: Quantifying the model structural error in carbon cycle data assimilation systems, Geosci. Model Dev., 6, 45–55, doi: 10.5194, gmd-6-45-2013, 2013.

Kuppel, S., Peylin, P., Maignan, F., Chevallier, F., Kiely, G., Montagnani, L., and Cescatti, A.: Model–data fusion across ecosystems: from multisite optimizations to global simulations, 7, 2581–2597, 2014.

Luo, Y. Q., Randerson, J. T., Abramowitz, G., Bacour, C., Blyth, E., Carvalhais, N., Ciais, P., Dalmonech, D., Fisher, J. B., Fisher, R., Friedlingstein, P., Hibbard, K., Hoffman, F., Huntzinger, D., Jones, C. D., Koven, C., Lawrence, D., Li, D. J., Mahecha, M., Niu, S. L., Norby, R., Piao, S. L., Qi, X., Peylin, P., Prentice, I. C., Riley, W., Reichstein, M., Schwalm, C., Wang, Y. P., Xia, J. Y., Zaehle, S., and Zhou, X. H.: A framework for benchmarking land models, 9, 3857–3874, https://doi.org/10.5194/bg-9-3857-2012, 2012.

MacBean, N., Maignan, F., Peylin, P., Bacour, C., Bréon, F.-M., and Ciais, P.: Using satellite data to improve the leaf phenology of a global terrestrial biosphere model, 12, 7185–7208, 2015.

MacBean, N., Peylin, P., Chevallier, F., Scholze, M., and Schürmann, G.: Consistent assimilation of multiple data streams in a carbon cycle data assimilation system, 9, 3569–3588, 2016.

MacBean, N., Bacour, C., Raoult, N., Bastrikov, V., Koffi, E. N., Kuppel, S., Maignan, F., Ottlé, C., Peaucelle, M., Santaren, D., and Peylin, P.: Quantifying and Reducing Uncertainty in Global Carbon Cycle Predictions: Lessons and Perspectives From 15 Years of Data Assimilation Studies with the ORCHIDEE Terrestrial Biosphere Model, submitted, n.d.

Migliavacca, M., Meroni, M., Busetto, L., Colombo, R., Zenone, T., Matteucci, G., Manca, G., and Seufert, G.: Modeling gross primary production of agro-forestry ecosystems by assimilation of satellite-derived information in a process-based model, 9, 922–942, 2009.

Moore, D. J., Hu, J., Sacks, W. J., Schimel, D. S., and Monson, R. K.: Estimating transpiration and the sensitivity of carbon uptake to water availability in a subalpine forest using a simple ecosystem process model informed by measured net CO2 and H2O fluxes, 148, 1467–1477, 2008.

Nave, L., Johnson, K., van Ingen, C., Agarwal, D., Humphrey, M., and Beekwilder, N.: International Soil Carbon Network (ISCN) Database v3-1, International Soil Carbon Network (ISCN), 2016.

Oberpriller, J., Cameron, D. R., Dietze, M. C., & Hartig, F. (2021). Towards robust statistical inference for complex computer models. Ecology Letters, 24(6), 1251-1261.

Papale, D., Reichstein, M., Aubinet, M., Canfora, E., Bernhofer, C., Kutsch, W., Longdoz, B., Rambal, S., Valentini, R., and Vesala, T.: Towards a standardized processing of Net Ecosystem Exchange measured with eddy covariance technique: algorithms and uncertainty estimation, 3, 571–583, 2006.

Parton, W. J., Schimel, D. S., Cole, C. V., and Ojima, D. S.: Analysis of factors controlling soil organic matter levels in Great Plains grasslands, 51, 1173–1179, 1987.

Peiro, H., Crowell, S., Schuh, A., Baker, D. F., O'Dell, C., Jacobson, A. R., Chevallier, F., Liu, J., Eldering, A., and Crisp, D.: Four years of global carbon cycle observed from the Orbiting Carbon Observatory 2 (OCO-2) version 9 and in situ data and comparison to OCO-2 version 7, 22, 1097–1130, 2022.

Peylin, P., Bousquet, P., Le Quéré, C., Sitch, S., Friedlingstein, P., McKinley, G., ... & Ciais, P. (2005). Multiple constraints on regional CO2 flux variations over land and oceans. Global Biogeochemical Cycles, 19(1).

Peylin, P., Law, R. M., Gurney, K. R., Chevallier, F., Jacobson, A. R., Maki, T., Niwa, Y., Patra, P. K., Peters, W., and Rayner, P. J.: Global atmospheric carbon budget: results from an ensemble of atmospheric CO 2 inversions, 10, 6699–6720, 2013.

Peylin, P., Bacour, C., MacBean, N., Leonard, S., Rayner, P., Kuppel, S., Koffi, E., Kane, A., Maignan, F., and Chevallier, F.: A new stepwise carbon cycle data assimilation system using multiple data streams to constrain the simulated land surface carbon cycle, 9, 2016.

Quaife, T., Lewis, P., De Kauwe, M., Williams, M., Law, B. E., Disney, M., and Bowyer, P.: Assimilating canopy reflectance data into an ecosystem model with an Ensemble Kalman Filter, 112, 1347–1364, 2008.

Randerson, J. T., van der Werf, G. R., Giglio, L., Collatz, G. J., and Kasibhatla, P. S.: Global Fire Emissions Database, Version 3 (GFEDv3. 1), Data set, Oak Ridge National Laboratory Distributed Active Archive Center, Oak Ridge, Tennessee, USA, 2013.

Raoult, N. M., Jupp, T. E., Cox, P. M., and Luke, C. M.: Land surface parameter optimisation through data assimilation: the ad-JULES system, Geosci. Model Dev. Discuss., doi: 10.5194, 2016.

Supprimé[Cédric Bacour]:

Raupach, M. R., Rayner, P. J., Barrett, D. J., DeFries, R. S., Heimann, M., Ojima, D. S., Quegan, S., and Schmullius, C. C.: Model–data synthesis in terrestrial carbon observation: methods, data requirements and data uncertainty specifications, 11, 378–397, 2005.

Rayner, P. J., Scholze, M., Knorr, W., Kaminski, T., Giering, R., and Widmann, H.: Two decades of terrestrial carbon fluxes from a carbon cycle data assimilation system (CCDAS), 19, 2005.

Ricciuto, D. M., King, A. W., Dragoni, D., and Post, W. M.: Parameter and prediction uncertainty in an optimized terrestrial carbon cycle model: Effects of constraining variables and data record length, 116, 2011.

Richardson, A. D., Williams, M., Hollinger, D. Y., Moore, D. J., Dail, D. B., Davidson, E. A., Scott, N. A., Evans, R. S., Hughes, H., and Lee, J. T.: Estimating parameters of a forest ecosystem C model with measurements of stocks and fluxes as joint constraints, 164, 25–40, 2010.

Sacks, W. J., Schimel, D. S., and Monson, R. K.: Coupling between carbon cycling and climate in a high-elevation, subalpine forest: a model-data fusion analysis, 151, 54–68, 2007.

Santaren, D., Peylin, P., Viovy, N., and Ciais, P.: Optimizing a process-based ecosystem model with eddy-covariance flux measurements: A pine forest in southern France, 21, 2007.

Santaren, D., Peylin, P., Bacour, C., Ciais, P., and Longdoz, B.: Ecosystem model optimization using in situ flux observations: benefit of Monte Carlo versus variational schemes and analyses of the year-to-year model performances, 11, 7137–7158, 2014.

Schimel, D. S., Braswell, B. H., Holland, E. A., McKeown, R., Ojima, D. S., Painter, T. H., ... & Townsend, A. R. (1994). Climatic, edaphic, and biotic controls over storage and turnover of carbon in soils. Global biogeochemical cycles, 8(3), 279-293.

Schimel, D., Stephens, B. B., & Fisher, J. B. (2015). Effect of increasing CO2 on the terrestrial carbon cycle. Proceedings of the National Academy of Sciences, 112(2), 436-441.

Schürmann, G. J., Kaminski, T., Köstler, C., Carvalhais, N., Vo\s sbeck, M., Kattge, J., Giering, R., Rödenbeck, C., Heimann, M., and Zaehle, S.: Constraining a land-surface model with multiple observations by application of the MPI-Carbon Cycle Data Assimilation System V1. 0, Geosci. Model Dev., 9, 2999–3026, gmd-9-2999-2016, 2016.

Sitch, S., Friedlingstein, P., Gruber, N., Jones, S. D., Murray-Tortarolo, G., Ahlström, A., Doney, S. C., Graven, H., Heinze, C., and Huntingford, C.: Recent trends and drivers of regional sources and sinks of carbon dioxide, 12, 653–679, 2015.

Stöckli, R., Rutishauser, T., Dragoni, D., O'keefe, J., Thornton, P. E., Jolly, M., Lu, L., and Denning, A. S.: Remote sensing data assimilation for a prognostic phenology model, 113, 2008.

Tarantola, A. (2005). Inverse problem theory and methods for model parameter estimation. Society for industrial and applied mathematics

Thum, T., MacBean, N., Peylin, P., Bacour, C., Santaren, D., Longdoz, B., Loustau, D., and Ciais, P.: The potential benefit of using forest biomass data in addition to carbon and water flux measurements to constrain ecosystem model parameters: case studies at two temperate forest sites, 234, 48–65, 2017.

Todd-Brown, K. E., Randerson, J. T., Post, W. M., Hoffman, F. M., Tarnocai, C., Schuur, E. A., & Allison, S. D. (2013). Causes of variation in soil carbon simulations from CMIP5 Earth system models and comparison with observations. Biogeosciences, 10(3), 1717-1736.

Trémolet, Y. (2006). Accounting for an imperfect model in 4D-Var. Quarterly Journal of the Royal Meteorological Society: A journal of the atmospheric sciences, applied meteorology and physical oceanography, 132(621), 2483-2504.

Vermote, E., Justice, C. O., and Bréon, F.-M.: Towards a generalized approach for correction of the BRDF effect in MODIS directional reflectances, 47, 898–908, 2008.

Wang, Y.-P., Leuning, R., Cleugh, H. A., and Coppin, P. A.: Parameter estimation in surface exchange models using nonlinear inversion: how many parameters can we estimate and which measurements are most useful?, 7, 495–510, 2001.

van der Werf, G. R., Randerson, J. T., Giglio, L., Collatz, G. J., Kasibhatla, P. S., and Arellano Jr, A. F.: Interannual variability in global biomass burning emissions from 1997 to 2004, 6, 3423–3441, 2006.

Williams, M., Richardson, A. D., Reichstein, M., Stoy, P. C., Peylin, P., Verbeeck, H., Carvalhais, N., Jung, M., Hollinger, D. Y., and Kattge, J.: Improving land surface models with FLUXNET data, 6, 1341–1359, 2009.

Wutzler, T. and Carvalhais, N.: Balancing multiple constraints in model-data integration: Weights and the parameter block approach, 119, 2112–2129, https://doi.org/10.1002/2014JG002650, 2014.

Zhu, C., Byrd, R. H., Lu, P., and Nocedal, J.: Algorithm 778: L-BFGS-B: Fortran subroutines for large-scale bound-constrained optimization, 23, 550–560, 1997.

Zobitz, J. M., Moore, D. J., Quaife, T., Braswell, B. H., Bergeson, A., Anthony, J. A., and Monson, R. K.: Joint data assimilation of satellite reflectance and net ecosystem exchange data constrains ecosystem carbon fluxes at a high-elevation subalpine forest, 195, 73–88, 2014.

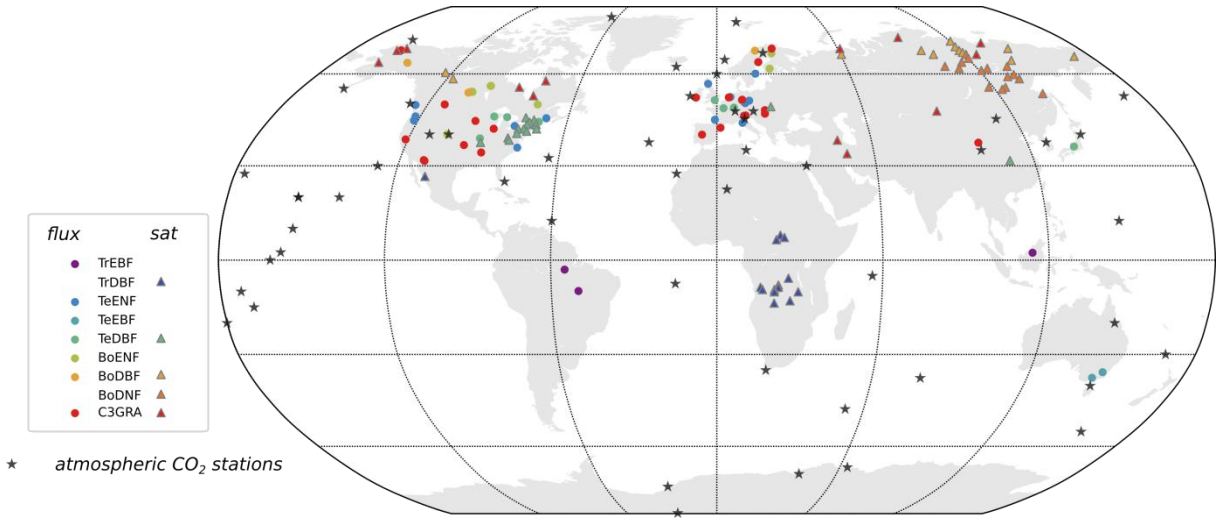

Figure 1: Location of the flux tower sites (circles), satellite pixels (triangles), and atmospheric CO_2 stations (black stars) used in this study.

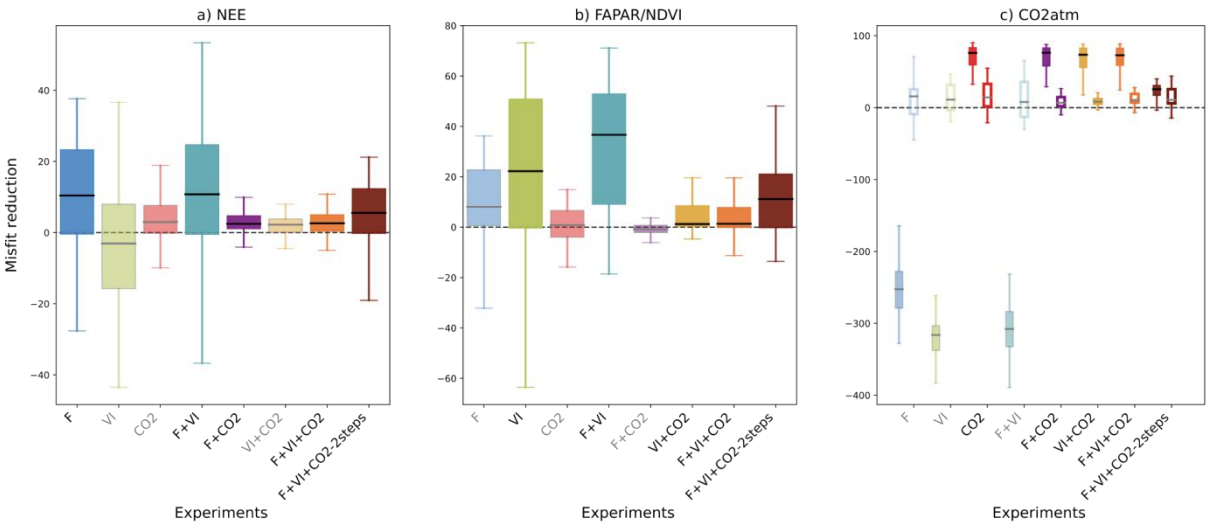

Figure 2: For all data streams, boxplots of the reduction of the model-data mismatch following the different assimilation experiments. For a given data stream, the assimilation experiments in which it is involved are labeled in black (x-axis) and the boxplot colors are dark colored; and in gray / light colors otherwise (back-compatibility check). For the atmospheric CO_2 concentration data at stations, the misfit reduction is calculated both for the raw (not detrended) data (left solid boxplot of each assimilation experiment, with colored boxplots) and the detrended data (right white boxplot of each assimilation experiment).

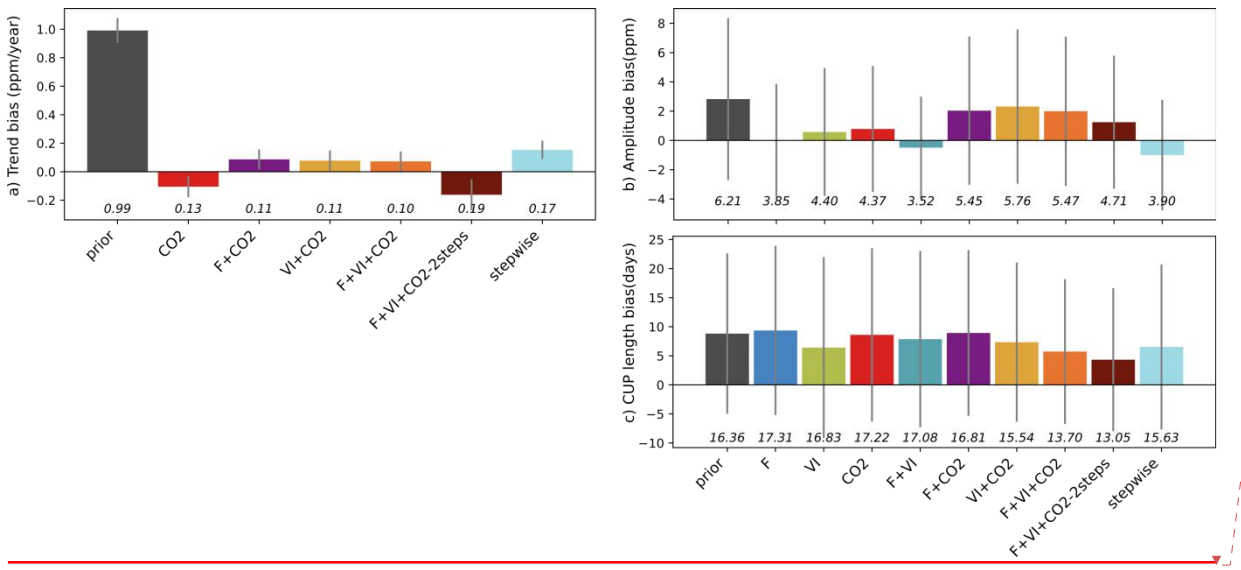

Figure 3: Residual biases of the atmospheric CO_2 time series between those measured at stations and the simulations (prior and optimized for each assimilation experiment), in terms of trend, magnitude of the seasonal cycle and length of the carbon uptake (CUP). The study results are compared to those obtained using a sequential approach (Peylin et al., 2016). The bars show for each quantity the mean bias relative to the measurements over the period 2000-2009. The standard deviations of the differences between observations and simulations over all stations are shown as the gray vertical lines, and the RMSD are provided below in italic.

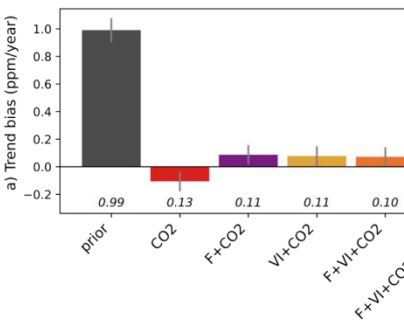

Supprimé[cbacour]:

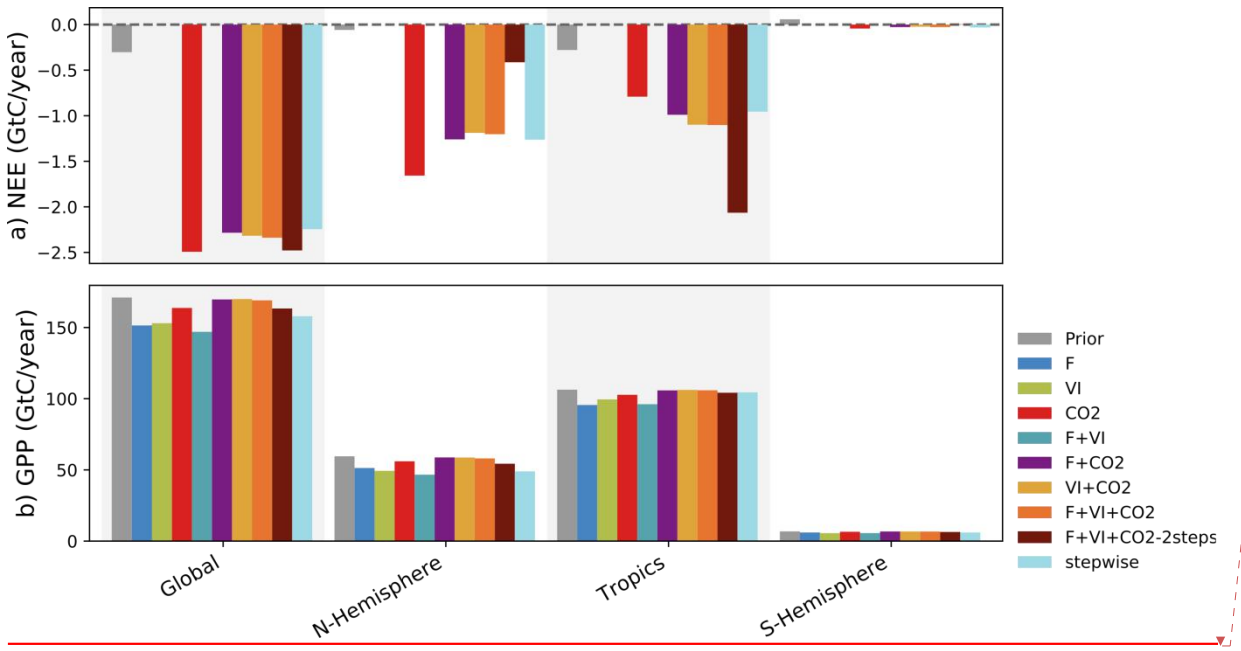

Figure 4: Global and regional C budget for NEE and GPP, and for the northern hemisphere (30°N-90°N), tropics (30°N-30°S) and southern hemisphere (30°S-90°S), regions, for the prior model and the model calibrated for the several assimilation experiments. For NEE, only the experiments involving atmospheric CO_2 data are shown. The period considered is 2000-2009.

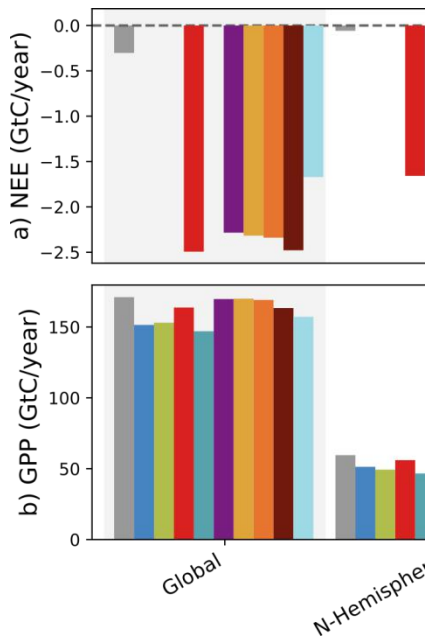

Supprimé[cbacour]:

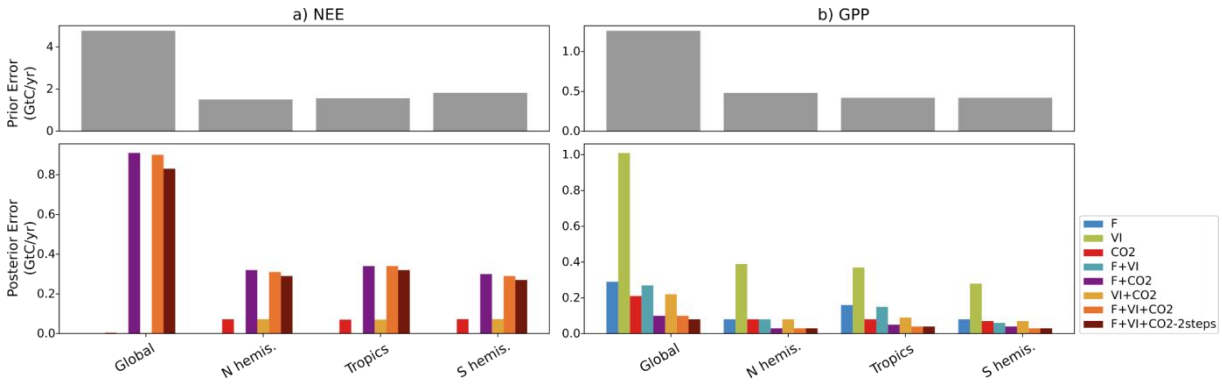

Figure 5: For NEE (left) and GPP (right) prior errors (top), and posterior errors obtained for each assimilation experiment (bottom), over the regions considered. For NEE, only the experiments involving atmospheric CO_2 data are shown.

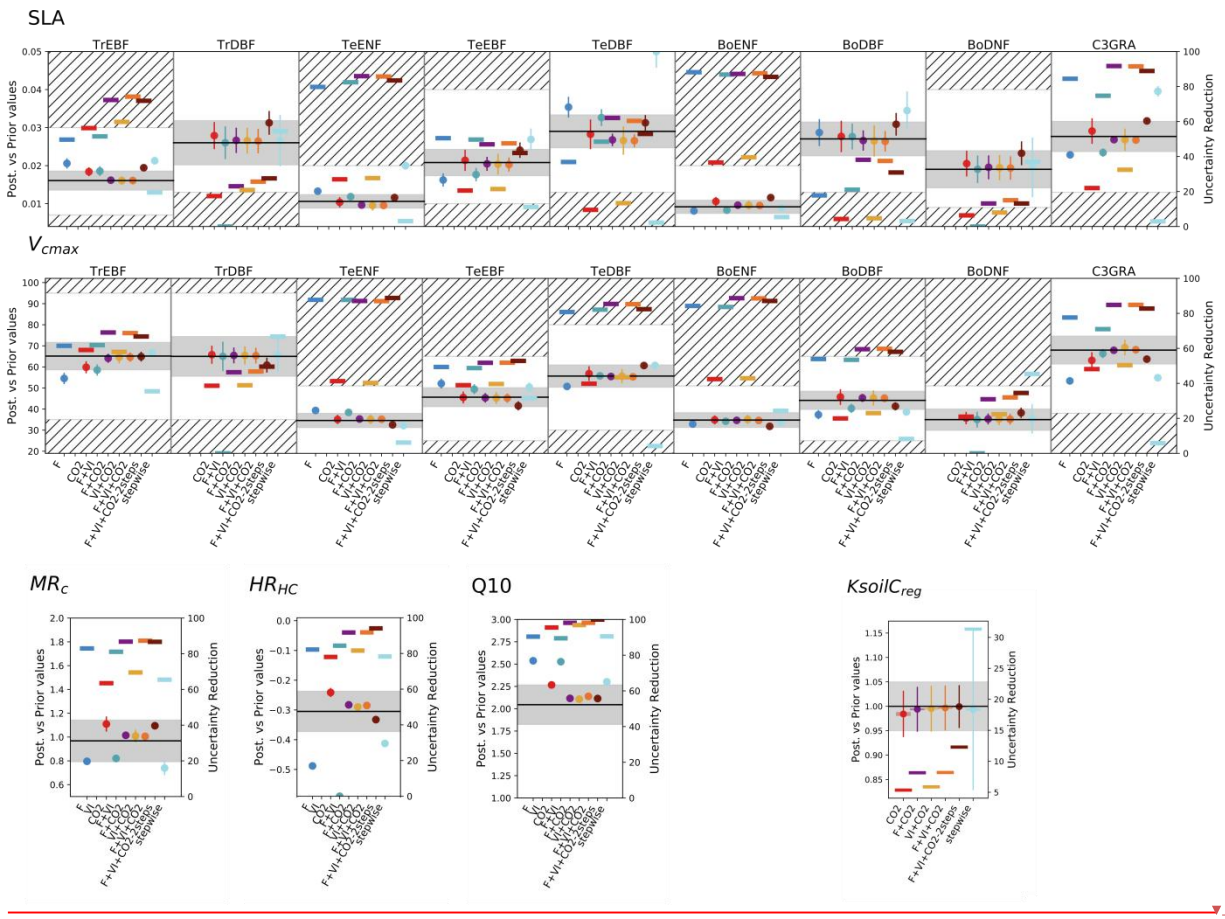

Figure 6: Prior and posterior parameter values and uncertainties for a set of optimized parameters (two PFT-dependent parameters - *SLA* and V_{cmax} - and four non-PFT dependent). The prior value is shown as the horizontal black line and the prior uncertainty (standard deviation) as the gray area encompassing it along the x-axis. For the PFT-dependent parameters, each box corresponds to a given PFT; empty boxes indicate that this parameter was not constrained for the corresponding PFTs. The white zone (non-dashed area) corresponds to the allowed range of variation. The optimized values are provided for each assimilation

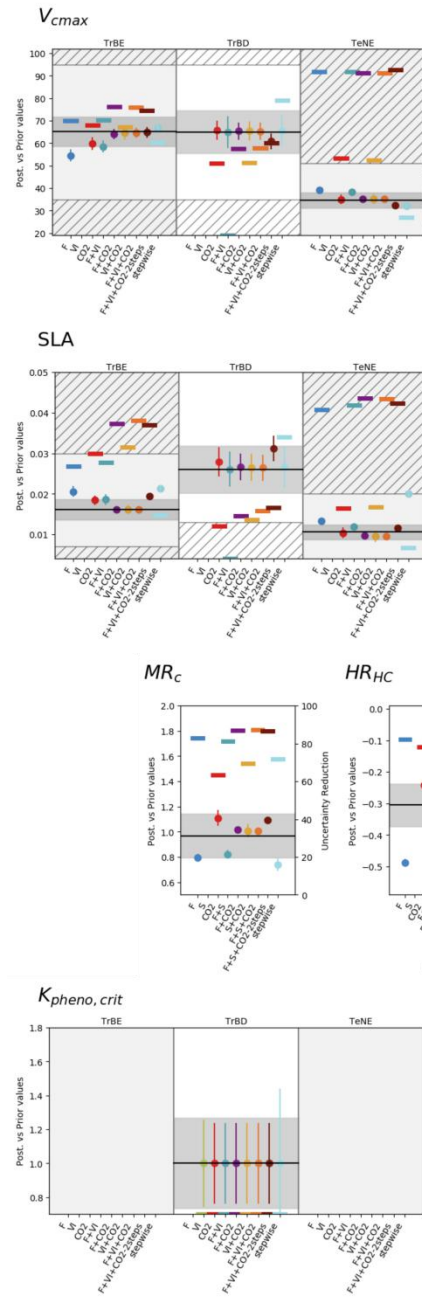

Supprimé[cbacour]:

Supprimé[cbacour]: **eight**

Mis en forme[cbacour]: Police: Italique

Mis en forme[cbacour]: Police: Italique

Mis en forme[cbacour]: Police: Italique, Indice

Mis en forme[cbacour]: Police: Italique

experiment (the eight ones considered in this study and the one from Peylin et al. (2016) – "stepwise"); the corresponding posterior errors are displayed as the vertical bars. Note that the prior values presented here are those used in this study, and not those of the stepwise (which are higher/lower for the photosynthesis and respiration / phenological parameters). For each assimilation experiment is also provided the uncertainty reduction (right y-axis) as the thick opaque horizontal bars. For *KsoilC_reg*, the posterior values displayed here correspond to the mean over the ecoregions (without Antarctica) considered; the semi-transparent horizontal bars on either side of the posterior values correspond to the standard deviation of the estimates.

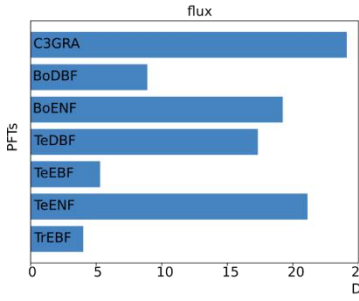

Supprimé[Cédric Bacour]:

Supprimé[Cédric Bacour]:

Supprimé[Cédric Bacour]: **Figure 7: Relative DFS for the F+VI+CO2 assimilation experiment. For Flux and Satellite data: relative DFS per PFT; for atmospheric CO_2 data: relative relative DFS (contribution) of the different stations to the fit.**

Name	Description	Data stream
Photosynthesis		
V_{cmax}	maximum carboxylation rate (µmol.m^{-2}.s^{-1})	F, CO2
$G_{s,slope}$	Ball-Berry slope	F, CO2
T_{opt}	optimal photosynthesis temperature (°C)	F, CO2
SLA	specific leaf area (m^2.g^{-1})	F, CO2
Soil water availability		
$H_{um,cste}$	root profile (m^{-1})	F, CO2
Phenology		
LAI_{MAX}	maximum LAI value	F, CO2
$K_{pheno,crit}$	multiplicative parameter of the threshold that determines the start of the growing season	F, VI, CO2
T_{senes}	temperature threshold for senescence (°C)	F, VI, CO2
$L_{age,crit}$	average critical age of leaves (days)	F, VI, CO2
$K_{LAI,happy}$	LAI threshold to stop using carbohydrate reserves	F, VI, CO2
Respiration		
Q10	temperature dependency of heterotrophic respiration	F, CO2
$HR_{H,c}$	Offset of the function for moisture control factor of heterotrophic respiration	F, CO2
MR_c	Offset of the affine relationship between temperature and maintenance respiration	F, CO2
$K_{soilC,site}$	Multiplicative factor of initial slow and passive carbon pools	F
$K_{soilC,reg}$	Multiplicative factor of initial slow and passive carbon pools	CO2

Table 1: List of the ORCHIDEE parameters to be optimized and data streams that constrain them (F for *in situ* flux measurements, VI for normalized satellite NDVI data, CO2 for atmospheric CO_2 concentration data).

experiment name	flux data	NDVI data	atmospheric CO_2 concentrations	number of optimized parameters	number of observations
F	**x**			133	150792
VI		**x**		19	149916
CO2			**x**	114	6360
F+VI	**x**	**x**		152	300708
F+CO2	**x**		**x**	182	157152
VI+CO2		**x**	**x**	114	156276
F+VI+CO2 **F+VI+CO2-2steps**	**x**	**x**	**x**	182	307068

Table 2: Characteristics of the various assimilation experiments (flux data – F, satellite NDVI vegetation index – VI, and atmospheric CO2 concentration – CO2).

	NEE	LE	VI	CO2
$\mathbf{R}$	1.75	1.75	0.33	1.22
$E\left[\mathbf{d}_{\mathbf{a}}^{\mathbf{o}}.\mathbf{d}_{\mathbf{b}}^{\mathbf{o}\,\mathrm{T}}\right]$	1.49	1.49	0.21	1.16
$ratio^{R}$	1.17	1.17	1.55	1.05
$\mathbf{H}_{\mathbf{o}}.\mathbf{B}.\mathbf{H}_{\mathbf{o}}^{\mathrm{T}}$	1.45	8.30	0.2	15.17
$E\left[\mathbf{d}_{\mathbf{b}}^{\mathbf{a}}.\mathbf{d}_{\mathbf{b}}^{\mathbf{o}\,\mathrm{T}}\right]$	0.92	5.45	0.24	6.29
$ratio^{B}$	1.59	1.52	0.83	2.41
$\mathbf{H}_{\mathbf{o}}.\mathbf{B}.\mathbf{H}_{\mathbf{o}}^{\mathrm{T}}+\mathbf{R}$	2.28	23.63	0.38	15.22
$E\left[\mathbf{d}_{\mathbf{b}}^{\mathbf{o}}.\mathbf{d}_{\mathbf{b}}^{\mathbf{o}\,\mathrm{T}}\right]$	1.75	22.11	0.31	6.39
$ratio^{BR}$	1.17	1.07	1.23	2.38
$\mathbf{H}_{\mathbf{o}}.\mathbf{A}.\mathbf{H}_{\mathbf{o}}^{\mathrm{T}}$	0.25	1.82	0.07	3.26
$E\left[\mathbf{d}_{\mathbf{b}}^{\mathbf{a}}.\mathbf{d}_{\mathbf{a}}^{\mathbf{o}\,\mathrm{T}}\right]$	-0.45	-5.12	-0.15	-2.13
$ratio^{A}$	-0.56	-0.36	-0.43	-1.53

Supprimé[cbacour]: <math>
Supprimé[cbacour]: <math>
Supprimé[cbacour]: <math>
Supprimé[cbacour]: <math>
Supprimé[cbacour]: <math>
Supprimé[cbacour]: <math>
Supprimé[cbacour]: <math>

Table 3: Consistency diagnostics of the error covariance matrices for the F (using NEE and LE data), VI, and CO2, assimilation experiments. The ratios are calculated with the mathematical expectation term as the denominator.

	OI		Relative DFS	
	1-step	**2-step**	**1-step**	**2-step**
flux	0.000586	0.000577	74.65	76.9
NDVI	0.000048	0.000048	11.12	11.68
CO2	0.002654	0.002035	14.23	11.42

Table 4: Observation influence and relative DFS statistics of each data stream for the joint assimilation experiments F+VI+CO2 and F+VI+CO2-2steps.

Supplementary Information for "Assimilation of multiple datasets results in large differences in regional to global-scale NEE and GPP budgets simulated by a terrestrial biosphere model"

Bacour C., MacBean N., Chevallier F., Léonard S., Koffi E.N., Peylin P.

Supplementary Text S1: Data assimilation experiments: differences with the stepwise approach

Although the stepwise assimilation has been extended to ten years of atmospheric CO_2 data (compared to only three years in Peylin et al. (2016)), there are few differences in the experimental set-up compared to the DA experiments considered in the present study: *i*) the set of optimized parameters is not strictly identical: the stepwise study did not optimize the parameters controlling the maximum LAI value per PFT nor the root profile, which are included in this study, but instead did include two additional parameters, one controlling the albedo of vegetation and the other reducing the hydric limitation of photosynthesis, which are not considered here; *ii*) for optimization of the phenology using satellite NDVI data, the C4 grass PFT was calibrated in Peylin et al. (2016), which is not the case in this study (MacBean et al., (2015) found that phenology for semi-arid PFTs was not well captured by the model and further improvements to the phenology schemes for these PFTs are needed).; i ii) the selection of the eddy-covariance sites is more selective in the present study (a few sites for which the model-data inconsistency was too important were discarded), which slightly reduces the number of site-years available for some PFTs; iv) finally, the *a priori* errors on model parameters (at the first and second steps) were set to 40% of the parameter variation range in Peylin et al. (2016), and were hence larger than what is prescribed in this study as a result of the consistency checks performed in Section 2.3.4.2.

Supplementary Text S2: Processing of atmospheric CO_2 data

In order to analyze the fit to the atmospheric CO_2 concentrations in terms of trend and seasonal cycle (magnitude and phase), the measured and modeled monthly time series are fitted using the CCGCRV package (ftp://ftp.cmdl.noaa.gov/user/thoning/ccgcrv/) following Thoning et al. (1989). It decomposes the time series into a first-order polynomial term (that represents the trend) and four harmonics, and then filters the residuals of that function in frequency space using a low-pass filter (cutoff frequency of 65 days). The seasonal cycle corresponds to the harmonics plus the filtered residuals. For a given time series, we calculate the magnitude of the seasonal cycle for each year as the difference between the maximum and minimum value, and the carbon uptake period (CUP) as the sum of the days when the values of the seasonal cycle extracted from the CO_2 concentration time series are negative (plant removing CO_2 from the atmosphere by convention) (Peylin et al., 2016). Examples of observed and

Supprimé[Cedric Bacour]: **different**

Mis en forme[Cedric Bacour]: Indice

Supprimé[Cedric Bacour]: T

Supprimé[Cedric Bacour]: DA

Supprimé[Cédric Bacour]: *i*) the study of Peylin et al. (2016) considers three years of atmospheric CO_2 data (from 2002 to 2004), while this study uses ten years of observations (2000-2009);

Supprimé[Cédric Bacour]: *i*

Supprimé[Cédric Bacour]: *i*

Supprimé[Cédric Bacour]: v

Mis en forme[Cédric Bacour]: Indice

simulated time series of atmospheric CO_2 concentrations at four sites are provided on Figure S1, as well as the corresponding trends derived by CCGCRV.

Mis en forme[Cedric Bacour]: Indice

Supplementary Text S3: Consistency diagnostics on the errors

Desroziers et al. (2005) tests

Several attempts were performed to specify the errors on model parameters in order to approach this goal considering each data-stream independently. With an initial definition of the parameter error corresponding to 40% of their variation range, the diagnostics on the **R** matrix, show a strong overestimation for all data streams (ratios about 3 for NEE and LE, 2 for NDVI and 12 for atmospheric CO_2), while the diagnostics on **B** were more consistent with ratios slightly higher than 1 but for NDVI (2.5). These results led us to revise the definition of **B** by decreasing the error for all parameters such that it corresponds to about 20% of the variation range for phenological parameters, and 12% for the other parameters (a value close to what was prescribed in Kuppel et al. (2013).

Reduced chi-square

For all experiments but those involving atmospheric CO2 measurements, the values of the reduced chi-square (after optimization) over all data are below 1 (Table S1), which corroborates the overestimation of the model-data and parameter errors observed previously. For fluxes and satellite data, this overestimation of the model-data error was expected, and even desired, given that the covariances in R were neglected by construction (off-diagonal elements set to zero). For CO2, the large value of χ^2 expresses a strong underestimation of the observation error not highlighted by the consistency diagnostics. Indeed, when determining $\mathbf{R_{CO2}}$, we purposely did not account for the structural error in ORCHIDEE that largely explains the strong bias between observed and simulated CO2 temporal profiles by about 1 ppm.yr^{-1}. This underestimation is even inflated in the joint assimilation experiments, even though the reduced chi-square over all data remains close to 1.

	Data - stream			
experiment	**F**	**VI**	**CO2**	**all data**
F	0.91			0.91
VI		0.78		0.78
CO2			8.57	8.57
F+VI	0.95	0.50		0.73
F+CO2	0.97		11.56	1.4
VI+CO2		0.74	11.72	1.18
F+VI+CO2	0.99	0.75	11.3	1.09
F+VI+CO2-2steps	0.96	0.67	7.88	0.97

Table S1: Values of the reduced chi-square determined after model calibration for the various assimilation

experiments, for each data-stream.

Supplementary Text S4: Optimisation performances

All optimizations but two (F and VI) reached a pre-defined maximum number of iterations (set to 35 for L-BFGS-B), therefore causing a hard stopping of the optimization (cf, Table S2, which also provides the values of the misfit functions for all assimilation experiments, relative to the background and to the observations). For the last iterations however, the variations of the misfit functions were low in all these cases, indicating that the final iterations were close to the minimum. The comparison between the observation and parameter terms of the posterior cost function shows how the total cost function is dominated by the weight of the model-data misfit.

The highest rate of change of the total cost function related to the observation term is obtained for the CO2 assimilation with a reduction of the misfit between model outputs and measurements by about 46. This is directly related to the correction of the large bias in the prior model with carbon pools at equilibrium relative to the prescribed prior error. Noticeably, the strong model improvement reached for CO2 comes with only a small variation in the model parameters as depicted by the posterior value of J_b. For the assimilation of the fluxes and satellite data alone (F and VI respectively), the model improvement is smaller, about 1.1, but shows a stronger departure of the parameters from their prior values compared to CO2 (Figure 3). The ratio of the norm of the gradient of the misfit function is also the highest for the CO2 experiment. On the opposite, it is slightly lower than one for VI which may indicate a possible issue of convergence towards the solution.

The two-step approach for the assimilation involving the three data-streams results in an enhanced agreement of the model with all data as compared to the one-step optimization. In parallel, the change in parameter values (departure from the background) is also higher for the two-step approach (Figure 3).

experiment	Number of iterations	Jo prior	Jo post	Jo prior/ Jo post (obs part)	Jo(F) post	Jo(CO_2) post	Jb post	Ratio norm grad J (prior/post)
F	34	75396	68305	1.10	68305		117.6	3.95
VI	29	65696	58517	1.12			37.9	0.94
CO2	35	1256783	27238	46.14		27238	7.8	759.5
F+VI	35	142118	108961	1.30	71353		79.3	0.97
F+CO2	35	1332190	109994	12.11	73232	36763	1.05	27.7
VI+CO2	35	1323494	92543	14.30		37257	1.3	132.3
F+VI+CO2	35	1398901	166797	8.39	74435	35918	1.6	168.7
F+VI+CO2-2steps	35	1398901	148206	9.43	72654	25002	44.6	-

Table S2: Characteristics of the various assimilation experiments: number of iterations, value of the cost functions related to the observation (Jo) and parameter terms (Jb) prior and posterior to the assimilation (as well as ratio of the posterior to prior values for Jo), ratio of norm of the gradient of the misfit functions (prior vs

posterior).

Supplementary Text S5: Analysis of the reduction of the model-data misfit

Mono-data stream assimilations

The increased consistency between model and flux data achieved after assimilation of F data is usually higher for NEE (median RMSD reduction of 10.4%, ranging from -69% to 38%) than for LE (0.3%; -42% / 28% range). This is largely explained by the higher number of optimized parameters related to the carbon cycle relative to the water cycle, and by the optimization of the multiplicative factor of the soil carbon pools that corrects the bias in the ecosystem respiration inherent to the model spin-up (Carvalhais et al., 2010; Kuppel et al. 2012). The strong model improvement for FAPAR in the VI assimilation (22.2% median; -32% / 36% range) follows a strong decrease of the simulated growing season length for deciduous PFTs in better accordance with the satellite observations, as discussed in MacBean et al. (2015). It mainly results from an earlier senescence for the several PFTs while the change of leaf onset depends on the type of vegetation. Both for the F and VI experiments, the reduction of the model-data misfit can be negative for some sites/pixels. This reflects how the assimilation may degrade the model performance at some sites/pixels by seeking for a common parameter set. This is not observed for atmospheric CO_2 data for which the optimized model is always closer to the observations than the prior model at all stations. Assimilating atmospheric CO_2 concentration measurements corrects the strong overestimation of the prior model (as also described in Peylin et al. (2016)), with a median RMSD reduction of 76% (ranging from 10% at HUN to 90% at SPO). This improvement corresponds to an increase of the net land carbon sink at the global scale in order to correct the strong mismatch between the observed trend and the *a priori* model. It is mainly realized by the optimization of the multiplicative factor of the soil carbon pools. As seen in Figure 2 from the detrended seasonal cycles of atmospheric CO_2 data (light red box), the changes in the modelled amplitude and phasing is smaller but still in better agreement with the observed data (median value of RMSD reduction of 14.4%; -21% / 55% range).

Multiple-data stream assimilations

The simultaneous assimilation of flux measurements and satellite NDVI data leads to enhanced model improvement as compared to when these data are assimilated alone: the median RMSD reductions are 10.8% for NEE (10.4% in the F case) and 36.7% for FAPAR/NDVI (22.2% in the VI case). In the simultaneous assimilations involving atmospheric CO_2 data, the most of the model improvement is attributed to CO2 while the benefit relative to fluxes and FAPAR/NDVI is weak: for NEE, the median RMSD reductions are only of 2.5% and 2.6% in the F+CO2 and F+VI+CO2 cases (as compared to 10% in the F case); for FAPAR, the median values are 1.2% and 1.4% for the VI+CO2 and F+VI+CO2 experiments

(22% in the VI case).

The 2-steps assimilation F+VI+CO2 results in a higher model improvement regarding both NEE and FAPAR (respectively 5.5% and 11.2%) than the one-step approach.

Regarding the raw atmospheric CO_2 data, the median improvements are 76.1% for CO2, 76.3% for F+CO2, 73.6% for VI+CO2, 72.9% for F+VI+CO2 and only 25.6% for F+VI+CO2-2steps.

More pronounced differences between experiments are obtained for the de-trended CO_2 time series: while the median RMSD reduction is of 14% in the CO2 experiment, it is decreased to 7.8% in F+CO2, 8.4% in VI+CO2, and 10.6% in F+VI+CO2; at the opposite the RMSD reduction is increased to 15.4% in F+VI+CO2-2steps.

Supplementary Text S6: Global budget and uncertainty reduction

For NEE, the global scale budget is about -2.4 GtC.yr^{-1} for all experiments using atmospheric CO_2 as a constraint: the lower value of -2.28 GtC.yr^{-1} is found for F+CO2; the higher values of -2.49GtC.yr^{-1} and -2.48 GtC.yr^{-1} are obtained for CO2 / F+VI+CO2-2steps.

In the northern and southern hemispheres, the CO2 assimilation results in the largest C sinks (-1.65 / -0.04 GtC.yr^{-1} for NH/SH) while the 2step assimilation induces the lowest one (-0.41 / 0.003 GtC.yr^{-1}); the opposite result is obtained in the southern hemisphere with lower (-0.79 GtC.yr^{-1}) / higher (-2.06 GtC.yr^{-1}) budgets found for CO2 / F+VI+CO2-2steps.

The reduction of the global scale GPP budget is respectively of -19.61 GtC.yr^{-1} and -17.91 GtC.yr^{-1} for the F and VI experiments, which correspond to the largest corrections obtained among the various assimilations considered.

The averaged change in GPP is about -7.33 GtC.yr^{-1} globally for the CO2 assimilation experiment. The corrections for the joint assimilations involving CO2 data is even lower: the mean global change are -1.07 GtC.yr^{-1} for VI+CO2, -1.35 GtC.yr^{-1} for F+CO2 and -1.98 GtC.yr^{-1} for F+VI+CO2. For the F+VI+CO2 2-step experiment, the constraint on GPP is close to that obtained when CO2 data are assimilated alone (-7.70 GtC.yr^{-1}).

For the joint assimilations, the posterior errors on NEE is about 0.9 GtC.yr^{-1} globally and about 0.3 GtC.yr^{-1} for the three regions considered. The lowest posterior errors on GPP are obtained for the two experiments that combine the three data streams (about 0.09 GtC.yr^{-1} at the global scale, and about 0.04 GtC.yr^{-1} depending on the region). The values are close to the ones obtained with F+CO2.

Supplementary Text S7: Relative constraints brought by the different datasets with respect to PFTs and atmospheric stations

We performed the analysis of the influence of each data stream by discriminating the influence of each PFT for flux and satellite data, and each station for atmospheric CO2 concentrations (Figure S3 - experiment F+VI+CO2). For the flux data, the results are mainly proportional to the number of observations available (hence, the lower results are obtained for BorDBF, TeDBF and TrEBF, for which the number of assimilated data is about one order of magnitude lower than for the other PFTs; see § 2.2.1).

For satellite NDVI data however, the number of data is the same for each PFT. The discrepancies between PFTs is thus less pronounced than for flux data and related to the ability of the selected parameters to correct the phenology of each PFTs (constrained by the NDVI data). For TrDBF and C3GRA, the inability to correct the start of the growing season (Kpheno,crit, remains close to the prior values, as seen in Figure 3) may explain the lower contribution of these PFTs.

For atmospheric CO_2 data, the DFS is relatively well distributed across stations, with a mean value of 1.9 (range 0.19 – 14.5), in particular in the northern hemisphere. The higher values are found for a few southern hemisphere stations: Halley Station - HBA (6), Syowa - SYO (8.4), South Pole - SPO (11.9) and Cap Grim Observatory - CGO (14.5). Possible reasons for their larger impact may combine: a strong *a priori* model-data mismatch that is substantially corrected, ocean-driven concentration variations not well captured by the prescribed ocean flux but incidentally well corrected by remote land fluxes, etc.

Mis en forme[Cedric Bacour]: Indice

Mis en forme[Cedric Bacour]: Police: Italique

Name	TropEBF^{F}	TropBRF^{VI}	TempENF^{F}	TempEBF^{F}	TempDBF^{F,VI}	BorENF^{F}	BorDBF^{F,VI}	BorDNF^{VI}	C3Grass^{F,VI}
Photosynthesis									
V_{cmax}	65 [35;95] *10*	65 [35;95] *10*	35 [19;51] *5.3*	45 [25;65] *6.7*	55 [30;80] *8.3*	35 [19;51] *5.3*	45 |25;65] *6.7*	35 [19;51] *5.3*	70 [38;102] *10.7*
$G_{s,slope}$	9 [6;12] *1*	9 [6;12] *1*	9 [6;12] *1*	9 [6;12] *1*	9 [6;12] *1*	9 [6;12] *1*	9 [6;12] *1*	9 [6;12] *1*	9 [6;12] *1*
T_{opt}	37 [29;45] *2.7*	37 [29;45] *2.7*	25 [17;33] *2.7*	32 [24;40] *2.7*	26 [18;34] *2.7*	25 [17;33] *2.7*	25 [17;33] *2.7*	25 [17;33] *2.7*	27.25 [19.2;35.2] *2.7*
SLA	0.0154 [0.007;0.03] *0.0038*	0.0260 [0.013;0.05] *0.0062*	0.0093 [0.004;0.02] *0.0027*	0.02 [0.01;0.04] *0.005*	0.026 [0.013;0.05] *0.0062*	0.0093 [0.004;0.02] *0.0027*	0.026 [0.013;0.05] *0.0062*	0.019 [0.009;0.04] *0.0052*	0.026 [0.013;0.05] *0.0062*
Soil water availability									
$H_{um,cste}$	0.8 [0.2;3] *0.47*	0.8 [0.2;3] *0.47*	1 [0.25;4] *0.62*	0.8 [0.2;3] *0.47*	0.8 [0.2;3] *0.47*	1 [0.25;4] *0.62*	1 [0.25;4] *0.62*	0.8 [0.2;3] *0.47*	4 [1;10] *1.5*
Phenology									
LAI_{MAX}	7 [4;10] *1*	7 [4;10] *1*	5 [3;8] *0.8*	5 [3;8] *0.8*	5 [3;8] *0.8*	4.5 [2.5;6.5] *0.7*	4.5 [2.5;6.5] *0.7*	3 [1.5;4.5] *0.5*	2.5 [1.5;3.5] *0.3*
$K_{pheno,crit}$		1 [0.7; 1.8] *0.18*			1 [0.7; 1.8] *0.18*		1 [0.7; 1.8] *0.18*	1 [0.7; 1.8] *0.18*	1 [0.7; 1.8] *0.18*
T_{senes}					12 [2;22] *3.3*		7 [-3;17] *3.3*	2 [-8;12] *3.3*	-1.375 [-11.4;9.4] *3.5*
$L_{age,crit}$	730 [490;970] *80*	180 [120;240] *20*	910 [610;1210] *100*	730 [490;970] *80*	180 [90;240] *25*	910 [610;1210] *100*	180 [90;240] *27.5*	180 [90;240] *27.5*	120 [30;180] *25*
$K_{LAI,happy}$	0.5 [0.35;0.7] *0.06*	0.5 [0.35;0.7] *0.06*	0.5 [0.35;0.7] *0.06*	0.5 [0.35;0.7] *0.06*	0.5 [0.35;0.7] *0.06*	0.5 [0.35;0.7] *0.06*	0.5 [0.35;0.7] *0.06*	0.5 [0.35;0.7] *0.06*	0.5 [0.35;0.7] *0.06*
Respiration									
Q10	1.9937 [1;3] *0.33*								
$HR_{H,c}$	-0.29 [-0.59;0.01] *0.1*								
MR_{c}	1 [0.5;2] *0.25*								
$K_{soilC,site}$	1 [0.5;2] *0.1*								
$K_{soilC,reg}$	1 [0.7;1.3] *0.1*								

Table S3: Prior value, interval of variation (in square brackets) and 1-sigma prior error (italic), of the optimized parameter. Except for those related to respiration, all parameters are PFT-dependent. The exponents F and VI associated to each PFT name indicate the availability of flux (F) and satellite (VI) data.

Figure S1: Monthly mean atmospheric CO_2 concentrations, for four stations (Mace Head - MHD (Ireland), Mauna Loa - MLO (Hawaii, USA) , Ryori - RYO (Japan), South Pole - SPO (Antarctic, USA)) over the period 2000–2009. The prior (blue) and the posterior (orange) model simulations are compared to the observations (black), and the corresponding RMSD is provided. The observation error is in grey. The dash lines correspond to the trend derived from the CCGCRV algorithm.

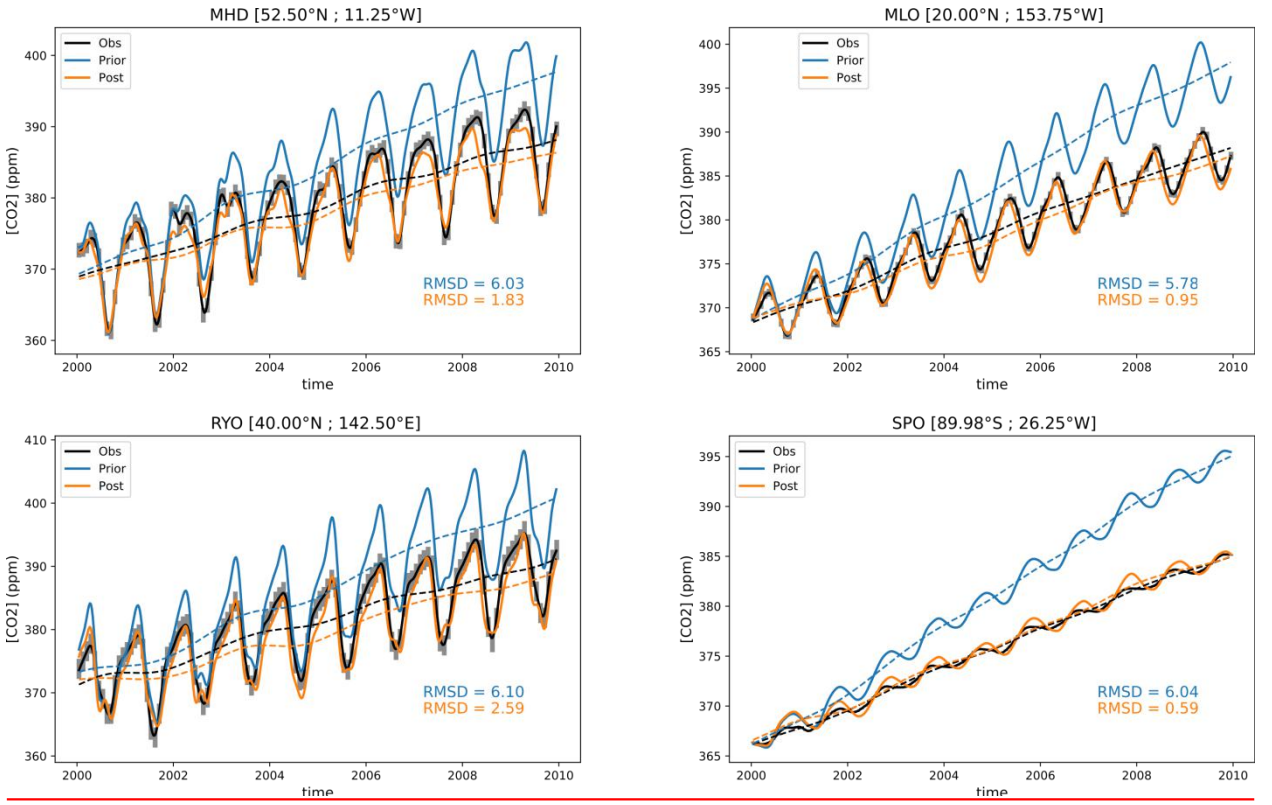

Figure S2: Prior and posterior parameter values and uncertainties for a set of optimized parameters (eight PFT-dependent parameters). The prior value is shown as the horizontal black line and the prior uncertainty (standard deviation) as the gray area encompassing it along the x-axis. For the PFT-dependent parameters, each box corresponds to a given PFT; empty boxes indicate that this parameter was not constrained for the corresponding PFTs. The white zone (non-dashed area) corresponds to the allowed range of variation. The optimized values are provided for each assimilation experiment ; the corresponding posterior errors are displayed as the vertical bars. Note that the prior values presented here are those used in this study, and not those of the stepwise (which are higher/lower for the photosynthesis and respiration / phenological parameters). For each assimilation experiment is also provided the uncertainty reduction (right y-axis) as the thick opaque horizontal bars.

Supprimé[Cedric Bacour]: **1**

Supprimé[Cedric Bacour]: **and four non-PFT dependent**

Supprimé[Cedric Bacour]: **(the eight ones considered in this study and the one from Peylin et al. (2016) – "stepwise")**

Supprimé[Cedric Bacour]: **For KsoilC_reg, the posterior values displayed here correspond to the mean over the eco-regions (without Antarctica) considered;**

Supprimé[Cedric Bacour]: **the semi-transparent horizontal bars on either side of the posterior values correspond to the standard deviation of the estimates**

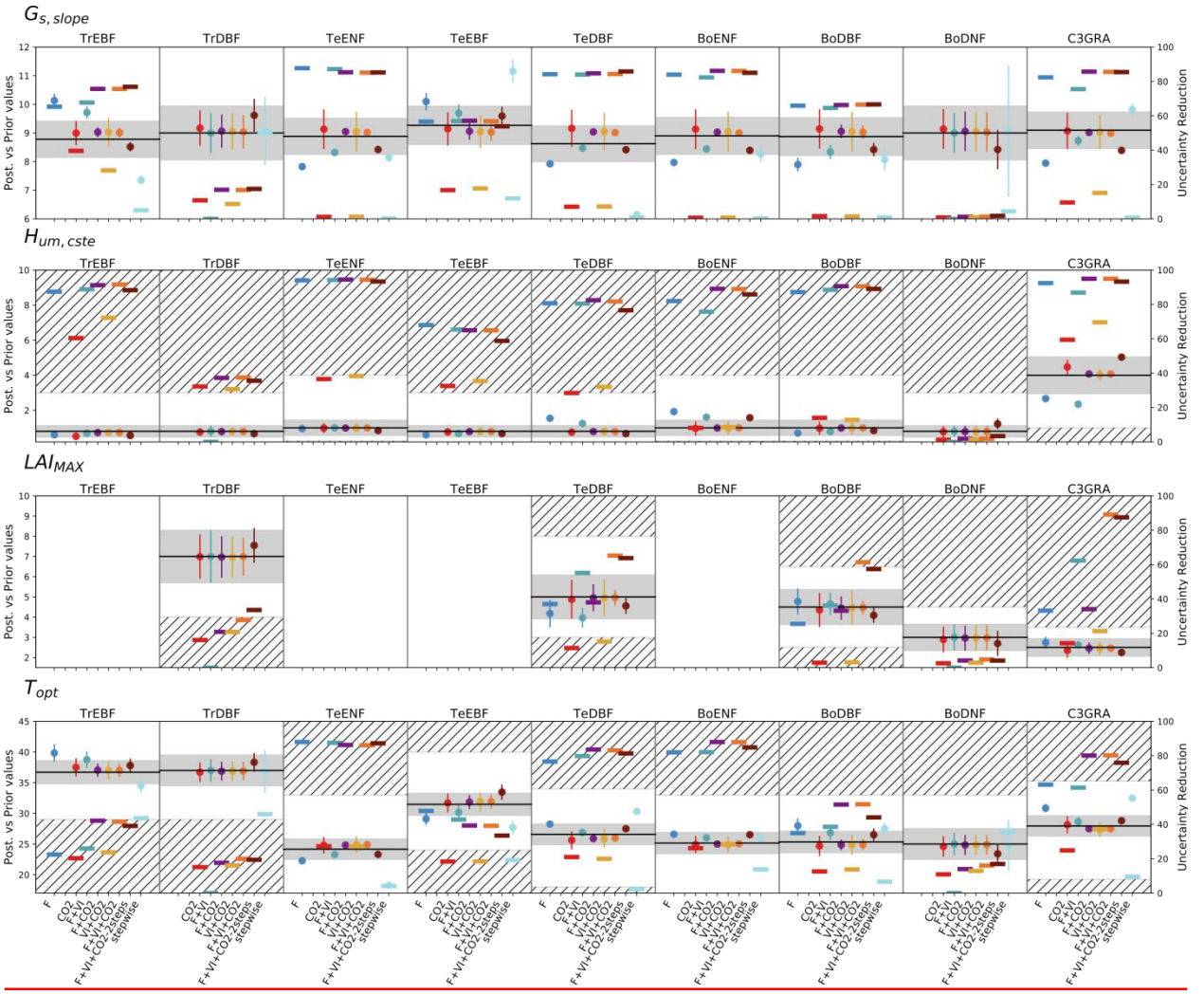
$G_{s,slope}$
$H_{um,cste}$
LAI_{MAX}
T_{opt}
TrEBF
TrDBF
TeENF
TeEBF
TeDBF
BoENF
BoDBF
BoDNF
C3GRA
Post. vs Prior values
Uncertainty Reduction
F
CO2
F+VI
F+CO2
VI+CO2
F+VI+CO2
F+VI+CO2 2steps
stepwise

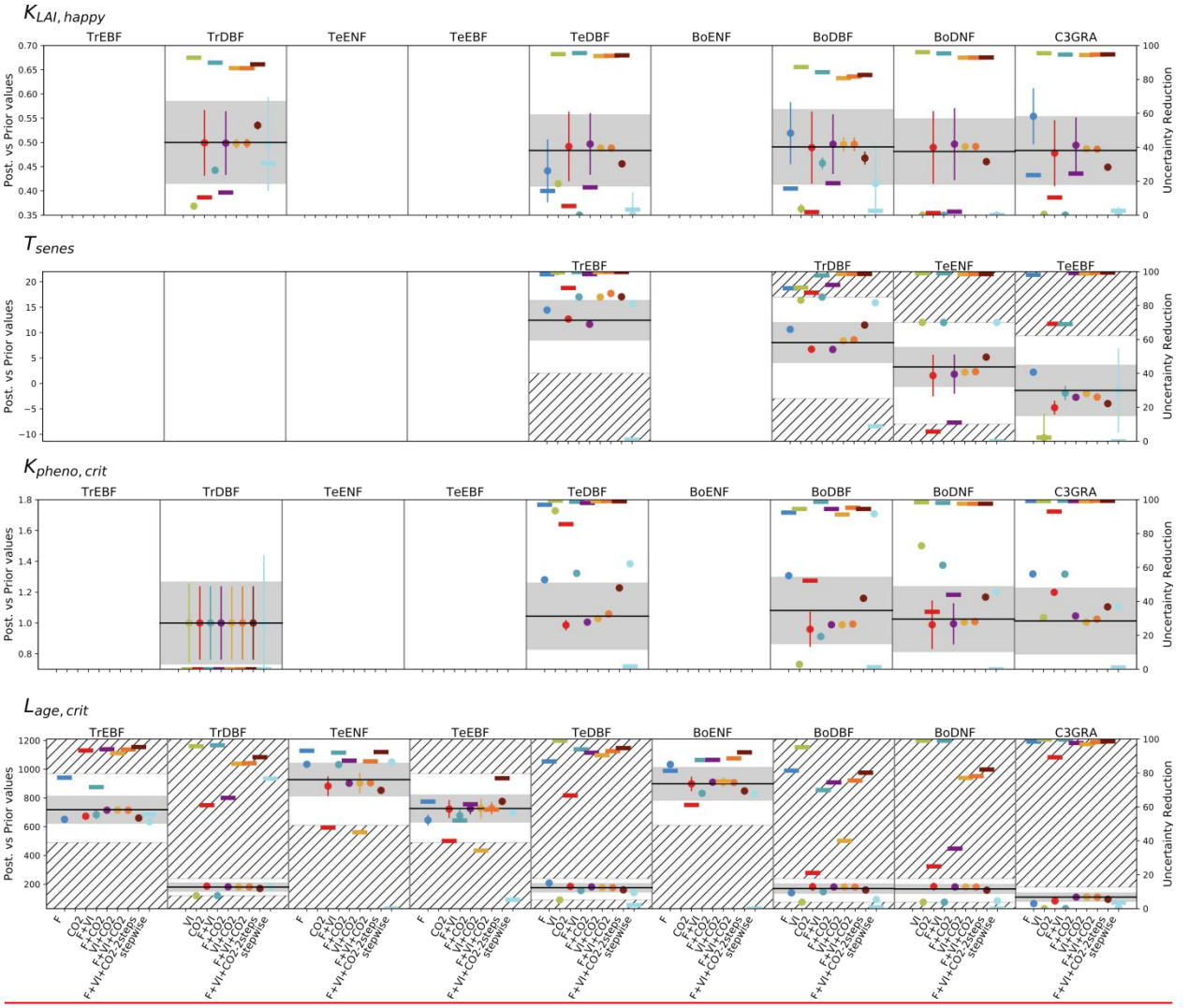

Figure S3: Relative DFS for the F+VI+CO2 assimilation experiment. For Flux and Satellite data: relative DFS per PFT; for atmospheric CO_2 data: relative relative DFS (contribution) of the different stations to the fit.

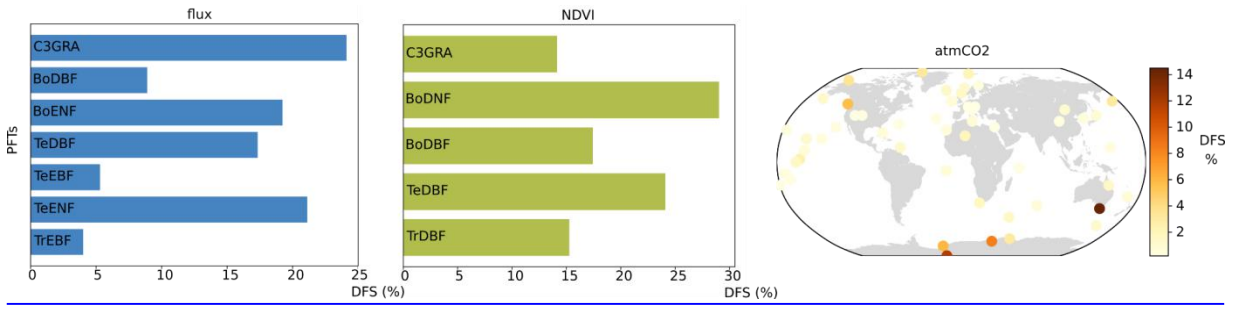

Mis en forme[Cedric Bacour]: Police: 10 pt, Gras

Mis en forme[Cedric Bacour]: Police: 10 pt, Gras

Mis en forme[Cedric Bacour]: Police: 10 pt, Gras, Indice

Mis en forme[Cedric Bacour]: Police: 10 pt, Gras

Supprimé[Cedric Bacour]:

References

Carvalhais, N., Reichstein, M., Ciais, P., Collatz, G. J., Mahecha, M. D., Montagnani, L., et al.:. Identification of vegetation and soil carbon pools out of equilibrium in a process model via eddy covariance and biometric constraints. *Global Change Biology*, *16*(10), 2813–2829, 2010.

Kuppel, S., Chevallier, F., & Peylin, P.: Quantifying the model structural error in carbon cycle data assimilation systems*, Geosci. Model Dev., 6, 45–55, doi: 10.5194*. gmd-6-45-2013, 2013.

Kuppel, Sylvain, Peylin, P., Chevallier, F., Bacour, C., Maignan, F., & Richardson, A. D.: Constraining a global ecosystem model with multi-site eddy-covariance data. *Biogeosciences*, *9*(10), 3757–3776, 2012.

MacBean, N., Maignan, F., Peylin, P., Bacour, C., Bréon, F.-M., & Ciais, P.: Using satellite data to improve the leaf phenology of a global terrestrial biosphere model. *Biogeosciences*, *12*(23), 7185–7208, 2015.

Peylin, P., Bacour, C., MacBean, N., Leonard, S., Rayner, P., Kuppel, S., et al.: A new stepwise carbon cycle data assimilation system using multiple data streams to constrain the simulated land surface carbon cycle. *Geoscientific Model Development (Online)*, *9*(9), 2016.

Thoning, K. W., Tans, P. P., & Komhyr, W. D.: Atmospheric carbon dioxide at Mauna Loa Observatory: 2. Analysis of the NOAA GMCC data, 1974–1985. *Journal of Geophysical Research: Atmospheres*, *94*(D6), 8549–8565, 1989.